

## FOREWORD

This report was prepared by the William H. Johnston Laboratories, Inc. under USAF Contract No. AF 33(616)-7678. The work was initiated under project No. 7360. "Chemistry and Physics of Materials" task No. 736003, "High Energy Materials Phenomena". The work was administered under the direction of the Directorate of Materials and Processes, Deputy for Technology, Aeronautical Systems Division with Mr. Stephen Zakanycz and Lt. Michael Charles as the project engineers.

This report covers work from 14 October 1960 to 14 December 1961. This is Part II which contains sections II and II. Report ASD-TDR-62-10 Part I will contain section I.

The authors particularly wish to thank those whose advice and council have proved so valuable in accomplishing the work described in this report. Although space prohibits mention of all contributors, we wish to acknowledge the following: G. Owen and W. S. Koski.

# *Contrails*

## ABSTRACT

The effects of radiation on any given material depends on the physics of the primary interaction with the material and the complex chemistry initiated.

In the present studies, the combination of a coincidence mass spectrometer (patented) and a special x-ray tube, which was described in Part I, has made possible direct measurements of the ion fragmentation patterns produced by x-ray impact on simple gas phase molecules. Mass spectra are reported for nitrous oxide, and for propane under bombardment by low energy x-rays (predominately aluminum  $K_{\alpha}$ ). For comparison purposes, spectra were also obtained of these materials under bombardment by 1200 ev primary electrons.

The present studies also concern measurements of the secondary electron energy distributions for a number of molecules of importance in radiation chemistry, at a fixed angle, using primary ionizing electrons in the energy range of 100 to 1000 ev. Measurement of the electron energy spectrum is accomplished in the coincidence mass spectrometer. Theoretical interpretation of the data in terms of radiation chemical effects is included.

The design, construction, and operation of the instrumentation, which has made these measurements possible, are described.

## PUBLICATION REVIEW

This technical documentary report has been reviewed and is approved.

FOR THE COMMANDER:



RICHARD J. VOSSLER, Capt. USAF  
Chief, Radiation Branch  
Physics Laboratory  
Directorate of Materials and Processes

TABLE OF CONTENTS

Section I

Ionic Fragmentation of Molecules by X-rays

M. Krause, M. Vestal, A. L. Wahrhaftig, F. W. Lampe, W. H. Johnston

	Page
I. GENERAL	
A. INTRODUCTION	1
B. ACCOMPLISHMENTS	1
II. THE COINCIDENCE MASS SPECTROMETER	2
A. PRINCIPLE OF OPERATION	2
B. DATA HANDLING	6
III. THEORETICAL CONSIDERATIONS	
A. FUNDAMENTAL RESEARCH NEEDS IN RADIATION EFFECTS ON MATERIALS	9
B. IONIZATION OF MOLECULES BY X-RADIATION	11
C. ION OPTICS	12
IV. DESIGN MODIFICATIONS AND CONSTRUCTION OF EXPERIMENTAL SYSTEM	15
A. INTRODUCTION	15
B. SPECIAL X-RAY TUBE	16
C. THE IONIZATION CHAMBER	16
D. THE GRID STRUCTURES	21
E. THE DRIFT TUBE AND ION DETECTOR	25
F. THE PUMPING SYSTEM AND SAMPLE HANDLING SYSTEM	26
G. THE TIME ANALYZER AND RELATED CIRCUITS	26
V. RESULTS AND CONCLUSIONS	30
A. CALIBRATIONS	30
B. PERFORMANCE TESTS	32
C. REAGENT MATERIALS AND ENERGY DISTRIBUTION OF BOMBARDING PARTICLES	32
D. ION DISTRIBUTION FROM BOMBARDMENTS WITH HIGH ENERGY ELECTRONS	34
E. INNER-SHELL IONIZATION AND ION FRAGMENTATION FROM BOMBARDMENTS WITH X-RAYS	36

TABLE OF CONTENTS (CONTINUED)

Section II

Secondary Electron Spectra from Bombardment of Gases with Electrons

M. Vestal, M. Krause, A. L. Wahrhaftig, W. H. Johnston

	Page
I. INTRODUCTION	41
II. THEORY OF THE IONIZING COLLISION OF ELECTRONS ON MOLECULES	41
III. EXPERIMENTAL PROCEDURE	45
IV. RESULTS	46
V. INTERPRETATION AND EVALUATION OF THE DATA	63
VI. CONCLUSIONS AND FUTURE RESEARCH	65
LIST OF REFERENCES	67

## LIST OF ILLUSTRATIONS

Figure		Page
1	Schematic Representation of the Coincidence Mass Spectrometer	3
2	Noise-to-Signal Ratio of Non-Coincidence and Coincidence Measurements	5
3	Block Diagram of Data Handling Systems: Visual Display Method; Multichannel Counting Method	7
4	Block Diagram of Data Handling System Using Multi-Channel Pulse Height Analyzer	8
5	Grid Structure With Voltages for Desired Ion Optics	14
6	Overall View of Experimental System	15
7	Ionization Chamber Showing, Left to Right Ion Drift Tube, Electrical Feedthrough Port, and Access Port to Electron Gun	17
8	Schematic Drawing of Ionization Chamber, Top View	18
9	Schematic Drawing of Ionization Chamber, Side View	19
10	Top View of Inside of Ionization Chamber	20
11	Grid Structure, Top View	22
12	Grid Structure, Side View	23
13	Photograph Showing Drift Tube, Ionization Chamber, and Pumping System of Coincidence Mass Spectrometer	25
14	Pumping System	27
15	Sample Handling System	27
16	Block Diagram of Time-To-Pulse-Height Converter	29
17	Section of Time-To-Pulse-Height Converter Showing Slightly Simplified Circuit Diagram of the Hold-On and Gate Circuit	29
18	Calibration Chart Relation Between Pressure in Sample Flask (Dubrovin Gauge) and Pressure in Ionization Chamber (Ionization Gauge)	30

## LIST OF ILLUSTRATIONS (CONTINUED)

Figure		Page
19	Calibration Chart of Pulse-Height Analyzer for a Preset Sawtooth of 8 $\mu$ sec. Length	31
20	Experimental Data as Obtained from Data Handling System	33
21	Spectrum of 1, 3-Butadiene with Nitrous Oxide under Electron Bombardment. Electron Energy 1200 ev.	35
22	Spectrum of Propane under Electron Bombardment Electrical Energy 1200 ev.	35
23	Spectrum of N <sub>2</sub> O under X-ray Bombardment	37
24	Spectrum of Propane under X-ray Bombardment	38
25	Vector Diagram of an Ionizing Collision	43
26	Calculated Differential Energy Spectrum of Secondary Electrons Ejected Perpendicular to the Primary Beam for Atomic Hydrogen at a Primary Electron Energy of 1000 ev.	44
27	Schematic Representation of the Coincidence Mass Spectrometer as Modified for Secondary Electron Energy Measurements	46
28	Integral Secondary Electron Spectra for N <sub>2</sub> Using 500 Electron Volt Primary Electrons	56
29	Integral Secondary Electron Spectra for N <sub>2</sub> Using 600 Electron Volt Primary Electrons, Results of Two Separate Runs	56
30	Integral Secondary Electron Spectra of Propane Using 400 Electron Volt Primary Electrons	57
31	Integral Secondary Electron Spectra of Propane Using 800 Electron Volt Primary Electrons	57
32	Secondary Electron Spectrum of N <sub>2</sub> Using 800 ev Primary Electron Energy	58
33	Secondary Electron Spectrum of N <sub>2</sub> Using 320 ev Primary Electron Energy	58
34	Secondary Electron Spectrum of Propane Using 320 ev Primary Electron Energy	59

## LIST OF ILLUSTRATIONS (CONTINUED)

Figure		Page
35	Secondary Electron Spectrum of Propane Using 1000 ev Primary Electron Energy	59
36	Secondary Electron Spectra of N <sub>2</sub> for Primary Electron Energy of 1000 ev	60
37	Secondary Electron Spectra of n-Butane for Primary Electron Energy of 1000 ev	60
38	Secondary Electron Spectra of 1, 3-Butadiene for Primary Electron Energy of 1000 ev	61
39	Secondary Electron Spectra of n-Pentane for Primary Electron Energy of 1000 ev	61
40	Secondary Electron Spectra of Argon for Primary Electron Energy of 1000 ev	62
41	Secondary Electron Spectra of Cyclohexane for Primary Electron Energy of 1000 ev	62
42	Calculated Integral Secondary Electron Spectrum for Atomic Hydrogen at a Primary Electron Energy of 1000 ev	64



## LIST OF TABLES

Table		Page
1	Mass Numbers from Primary and Secondary Reactions	39
2	Materials Used in Secondary Electron Spectra Measurements	47
3	Secondary Electron Energy Spectrum for N <sub>2</sub> Using 320 ev Primary Electron Energy	48
4	Secondary Electron Spectrum for N <sub>2</sub> Using 800 ev Primary Electron Energy	49
5	Secondary Electron Energy Spectrum for Propane Using 320 ev Primary Electron Energy	50
6	Secondary Electron Energy Spectrum for Propane Using 800 ev Primary Electron Energy	51
7	Secondary Electron Energy Spectrum for N <sub>2</sub> Using 1000 ev Primary Electron Energy	52
8	Secondary Electron Energy Spectrum for Argon Using 1000 ev Primary Electron Energy	52
9	Secondary Electron Energy Spectrum for Propane Using 1000 ev Primary Electron Energy	53
10	Secondary Electron Energy Spectrum for n-Butane Using 1000 ev Primary Electron Energy	53
11	Secondary Electron Energy Spectrum for n-Pentane Using 1000 ev Primary Electron Energy	54
12	Secondary Electron Energy Spectrum for 1, 3 Butadiene Using 1000 ev Primary Electron Energy	54
13	Secondary Electron Energy Spectrum for Cyclohexane Using 1000 ev Primary Electron Energy	55
14	Fraction of Secondary Electrons Exceeding the Ionization Potential of the Molecule for 1000 ev Primary Electron Energy	63

# *Contrails*

Section I. IONIC FRAGMENTATION OF MOLECULES  
BY X-RAYS

A. INTRODUCTION

The orderly development of our understanding of radiation-induced chemical change requires information on the macroscopic effects of radiation, and on the detailed mechanisms and elementary processes which produce these effects. While it is evident that further information, experimental and theoretical, is needed in all phases of this field, this need is particularly acute in regard to detailed molecular information on the primary processes induced by high energy ionizing radiation. At the present time, information on the elementary processes induced by x-rays is lacking.

In the present research program the Coincidence Mass Spectrometer (patented) was used. This instrument, available only at William H. Johnston Laboratories, Inc., has made possible a unique experimental program. In this instrument, a molecule of interest was ionized with an energetic electron or with an x-ray. The resulting ion, or ion fragment, was detected in delayed coincidence with the corresponding secondary electron. The ion was identified by this delay time.

The purpose of this project was to obtain new fundamental data on certain primary processes in radiation chemistry. This knowledge is needed to correlate and to extend current theories toward a better basic understanding of radiation effects on materials. The primary processes under study were inner-shell ionization of molecules by x-radiation and secondary electron emission following electron impact.

Several studies are described which were conducted with this experimental system during the period of the present report. Among these were the processes induced by low energy x-rays and the ion distribution produced by such bombardment. Also presented are the conditions of the gas phase irradiations of the simple molecules, and the data derived from these experimental measurements.

B. ACCOMPLISHMENTS

An early version of the Coincidence Mass Spectrometer has been modified for the studies of ionization processes under x-ray bombardment. The stringent and difficult problems involved in this investigation required major changes in design and construction. A special x-ray tube developed for these studies is described in Part I. The use of the x-rays for irradiation required special grid structures and ion detectors. An improved system was designed and built for data handling.

Manuscript released for publication 1 December 1961 as an ASD Technical Report.

The entire Coincidence Mass Spectrometer has been thoroughly tested and calibrated, particularly in regard to the investigation of the fragmentation patterns of gases under x-ray bombardment. Comparative measurements were made using electrons as bombarding particles. Also provision has been made to make possible investigations that employ other ionizations such as ultra-violet radiation.

The performance of the spectrometer has been proven in measurements on a number of simple gases. Spectra were obtained for nitrous oxide, nitrogen, butadiene, and propane under electron and x-ray bombardments. Differences in the patterns of fragmentation were observed between x-ray and electron bombardment. Theoretical mechanisms are discussed for these processes. Data are interpreted in terms of the decomposition of multiply charged primary ions.

## II. THE COINCIDENCE MASS SPECTROMETER

### A. PRINCIPLE OF OPERATION

The importance of the Coincidence Mass Spectrometer to the present measurements has been described in Chapter I. This unique instrument represents the first application of the coincidence principle to mass spectrometry.

A schematic representation of the Coincidence Mass Spectrometer is presented in Figure 1. In operation the sample enters the ionization chamber where an electron from the electron gun or an x-ray photon from the x-ray tube collides with a molecule, in this case a low-mass paraffinic hydrocarbon, between grids G1 and G2. When this collision results in ionization of the molecule, the secondary electron is collected very rapidly to produce a pulse in the electron detector. The corresponding positive ion is accelerated through the remaining grids and drifts through the evacuated ion drift tube, finally producing a pulse in the ion detector. The time which elapses between the electron pulse and the corresponding ion pulse is a measure of the mass-to-charge ratio of the ion. Thus the heavier the ion the longer it takes to arrive at the ion detector following the very fast collection of the electron.

The advantages of this coincidence mass spectrometer are many. Foremost among them is the great sensitivity of this instrument. Conventional mass spectrometers consist chiefly of the magnetic separator type or of the pulsed time-of-flight variety. The use of the coincidence principle gives a greatly increased sensitivity which makes possible the present measurement of ion fragmentation by inner shell x-ray ionization.

Furthermore, the instrument lends itself to a unique measurement, namely, the determination of ion charge. The differential arrival time of each electron and its corresponding ion uniquely defines the mass-to-charge ratio of the ion. The repeated measurement of the pulse heights of an ion gives a distribution function which defines the charge of the ion. The ability to measure the multiplicity of charge of the ion is, obviously, most valuable to the x-ray study.

# COINCIDENCE MASS SPECTROMETER

*Contrails*

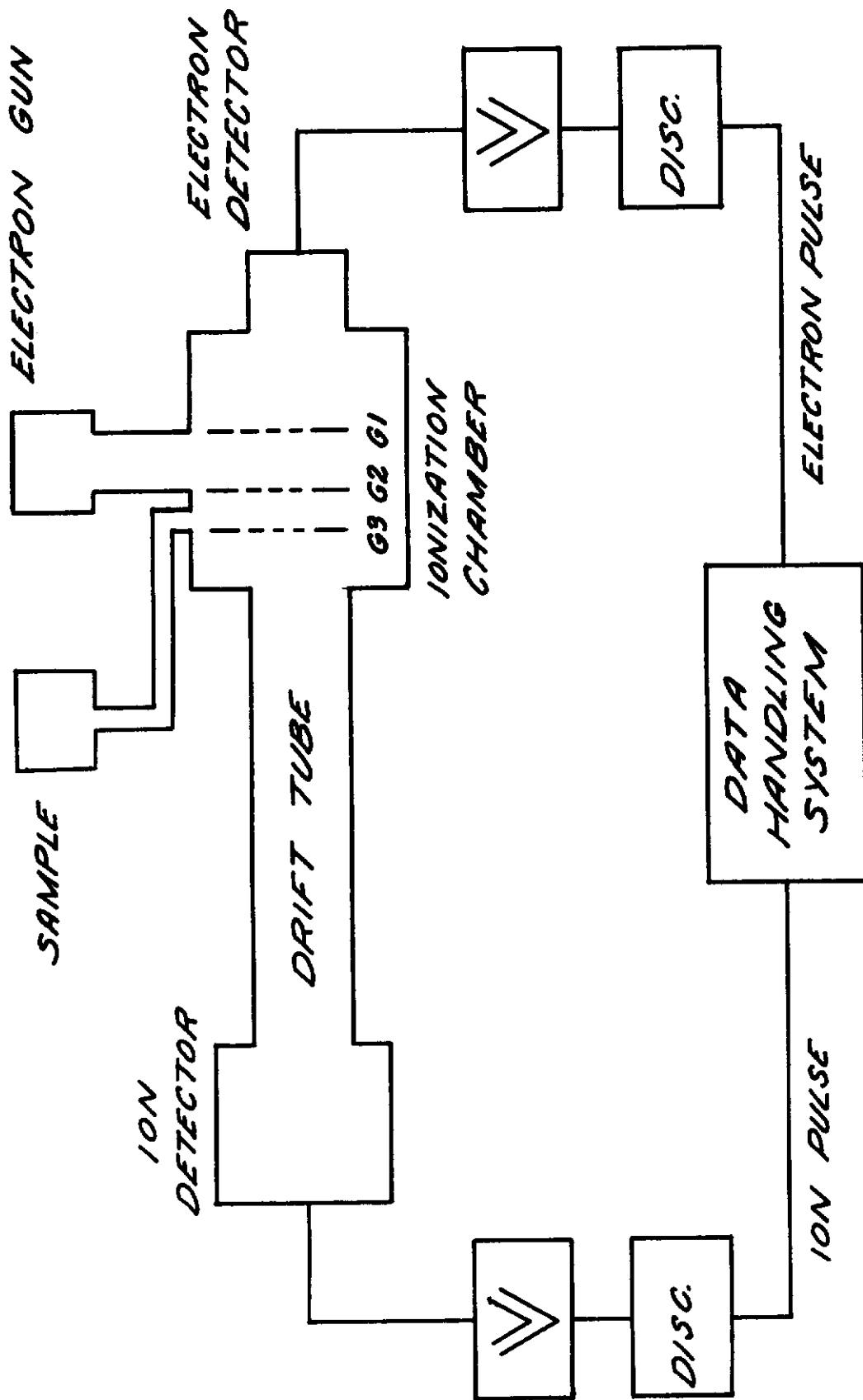


Figure 1 Schematic Representation of the Coincidence Mass Spectrometer.

# Contrails

The high sensitivity of the Coincidence Mass Spectrometer is due to reduction of the noise level accomplished by the use of the coincidence principle. In the Coincidence Mass spectrometer the ratio of random coincidence or "noise" to time coincidence signal is given by

$$\frac{N_R}{N_C} = \frac{\tau N_p [F_e + N_e/N_p + N_N/N_p] [(1-F_e)F_I + N_N/N_p]}{F_e F_I} \quad (1)$$

where  $N_R$  is the ratio of random or "noise" coincidence,  $N_C$  is the time coincidence signal rate;  $\tau$  is the time interval per unit mass for the delayed coincidence measurements;  $N_p$  is the rate at which ionization process occur in the ionization chamber;  $F_e$  and  $F_I$  are the collection efficiencies for secondary electrons and ions, respectively;  $N_e$  is the rate of "stray" or scattered electrons detected; and  $N_N$  is the rate of purely random noise pulses on the electron multiplier detectors.

The greatly increased sensitivity resulting from the application of the coincidence principle is shown graphically in Figure 2. The parameter values used in this illustration are as follows:

Time Interval/unit mass, $\tau$	$2 \times 10^{-7}$ sec.
Electron Collection Efficiency, $F_e$	90%
Ion Collection Efficiency, $F_I$	90%
Ratio of Stray Electrons to Ionization Processes, $N_e/N_p$	1.0
Random Noise Rate on Multipliers, $N_N$	1/sec.

In Figure 2 the ratio of random, "noise" coincidence to time coincidence signal,  $N_R/N_C$ , is plotted against the rate of ionization events,  $N_p$ , as given by Equation (1) using the parameter values listed above. For similar non-coincidence the noise to signal ratio is simply

$$\frac{N}{S} = \frac{N_N}{F_I N_p} \quad (2)$$

where  $N/S$  is the noise-to-signal ratio, and  $N_N$ ,  $F_I$ , and  $N_p$  are the detector random noise rate, ion collection efficiency, and ionization rate, respectively, as in Equation (1). For comparison the noise to signal ratio of non-coincidence measurements is also plotted in Figure 2 for the same parameter values.

The range of signal levels attainable in the x-ray ionization and fragmentation studies will generally be in the region below 100 counts per second. This conclusion is valid for the special x-ray tube designed for these studies. For commercially available x-ray tubes the signal levels are much lower. From Figure 2 it can be seen that at a total signal level of one count per second, the Coincidence Mass Spectrometer gives a reduction in noise level of a factor of more than  $10^6$  over the non-coincidence measurements. Thus at this extremely low total signal level, fragment ions which contribute as little as  $10^{-5}$  of the total level are measurable at a signal level which is still ten times the noise level. It is this extremely high sensitivity to very low signal rates which results from the reduction of the background noise through applications of the coincidence principle that makes the measurement of x-ray ionization possible.

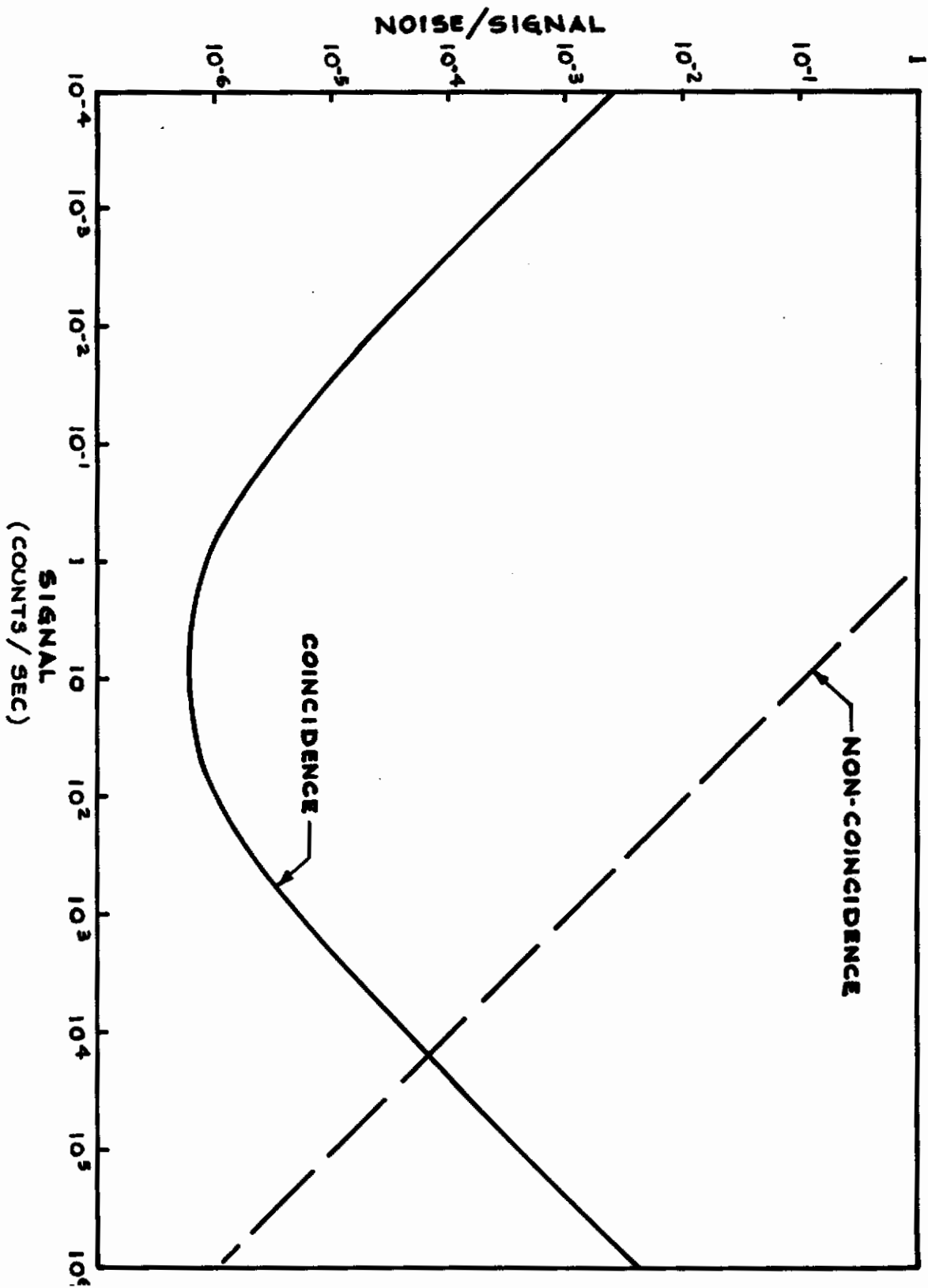


Figure 2 Noise to Signal Ratio of Non-coincidence and Coincidence Measurements.

## B. DATA HANDLING

The primary experimental information consists of the arrival of an electron pulse and the subsequent arrival of the corresponding ion pulse. The correlation of these two sets of signals is done in either of three available systems. The first two systems, which are briefly described below, were the previous approaches to the problem; these are still useful for certain applications. The third system is the fastest method and was used almost exclusively for these studies.

The first system was the visual display method. It is shown in Figure 3, Part A. In this system the electron pulse triggers a horizontal sweep generator and the amplified ion pulse produces a vertical oscilloscope deflection. Thus, for a left to right horizontal sweep, the distance to the right is a measure of the relative mass of the ion. Actually the arrival of an ion (and, therefore, the distance along the horizontal sweep) is proportional to the square root of the mass number of the ion (for ions of the same charge). Thus in Figure 3 the mass of the ion,  $\tau_2$ , is approximately 4 times the mass of the ion,  $\tau_1$ .

The second system or counting method for data handling is shown in Figure 3, part B. In this method the electron pulses are delayed by a series of transistorized delay circuits and placed in coincidence with the ion pulses by means of a series of "and" gates. These gates in turn feed a series of scaler channels in a multi-channel digital scaler. In operation each channel is set for a given mass number. All channels are operated simultaneously and the counting rate at each mass number is obtained from the appropriate scaler channel.

It should be pointed out that this method reduces the number of accidental coincidences because of the narrow time window in which coincidences are permitted. One drawback is the slow scanning of the total spectrum, step by step. Thus any fluctuations or shifting of amplifications, voltages, or pressures will influence the relative abundances of the mass fragments.

The third data handling system is essentially free from the fluctuations and changes of a long analysis. This system is shown in Figure 4; it utilizes a 256 channel memory core pulse height analyzer and provides high data resolution covering the entire range of electron-to-ion analysis times. In this method the electron pulse and its corresponding ion pulse produce a single converted pulse whose height is proportional to the difference in the arrival times of the ion and electron pulses. In operation, the succession of output pulses from this converter are fed directly to the 256 channel pulse height analyzer.

Following a period of analysis, the data which consists of a number of counted pulses in each of the channels are either printed in digital form or graphed on a pen recorder. This system of data handling is the most sophisticated of the three described. In principle, this system corresponds to the first method. The sophisticated circuit, however, allows the display and preservation of the entire spectrum quantitatively in one simple automatic operation.



# DATA HANDLING SYSTEM

## A) VISUAL DISPLAY

## B) COUNTING DEVICE

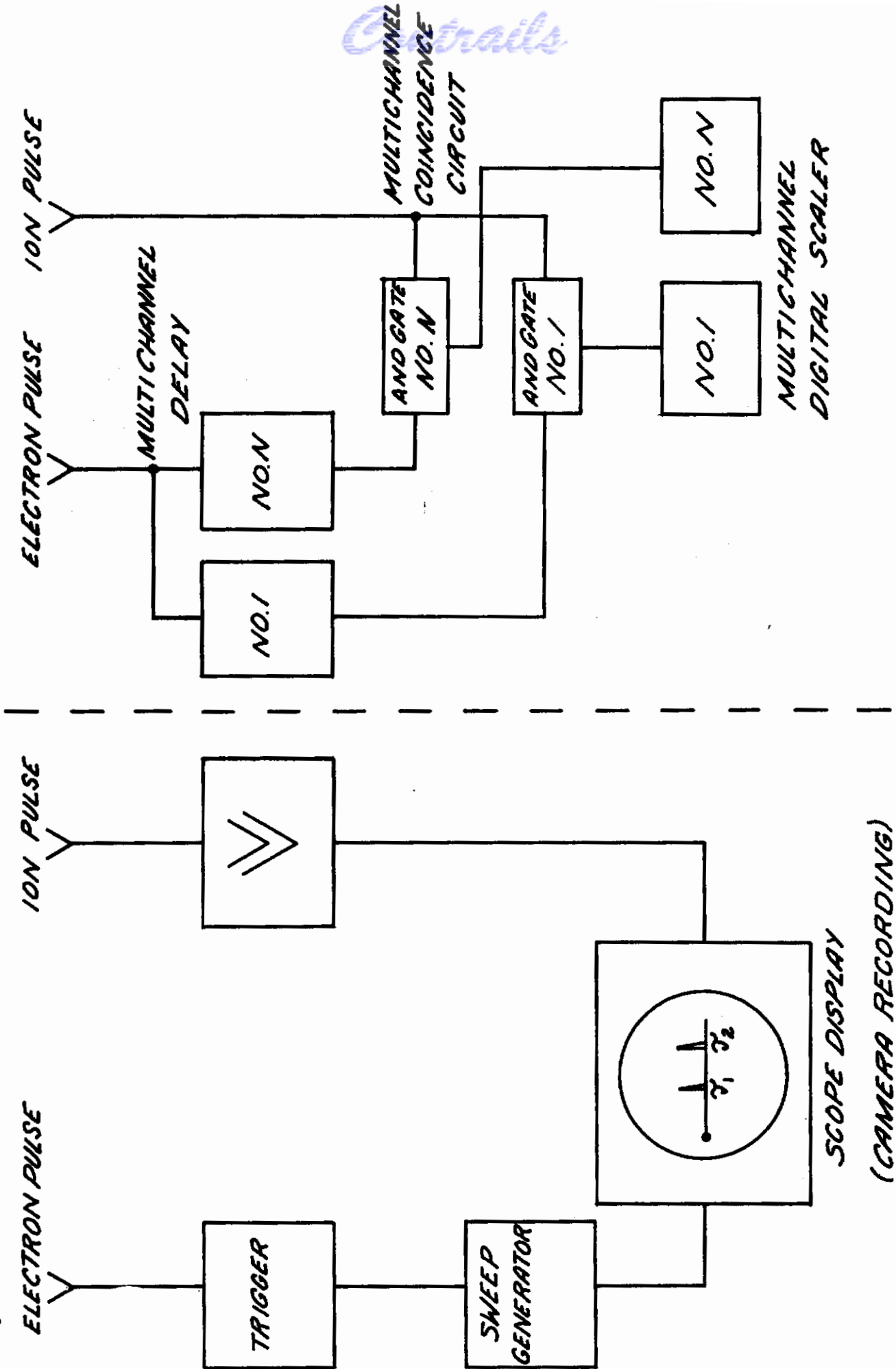


Figure 3 Block diagram of data handling systems: visual display method; multichannel counting method.

DATA HANDLING SYSTEM

C) ADAPTED PULSE HEIGHT ANALYZER

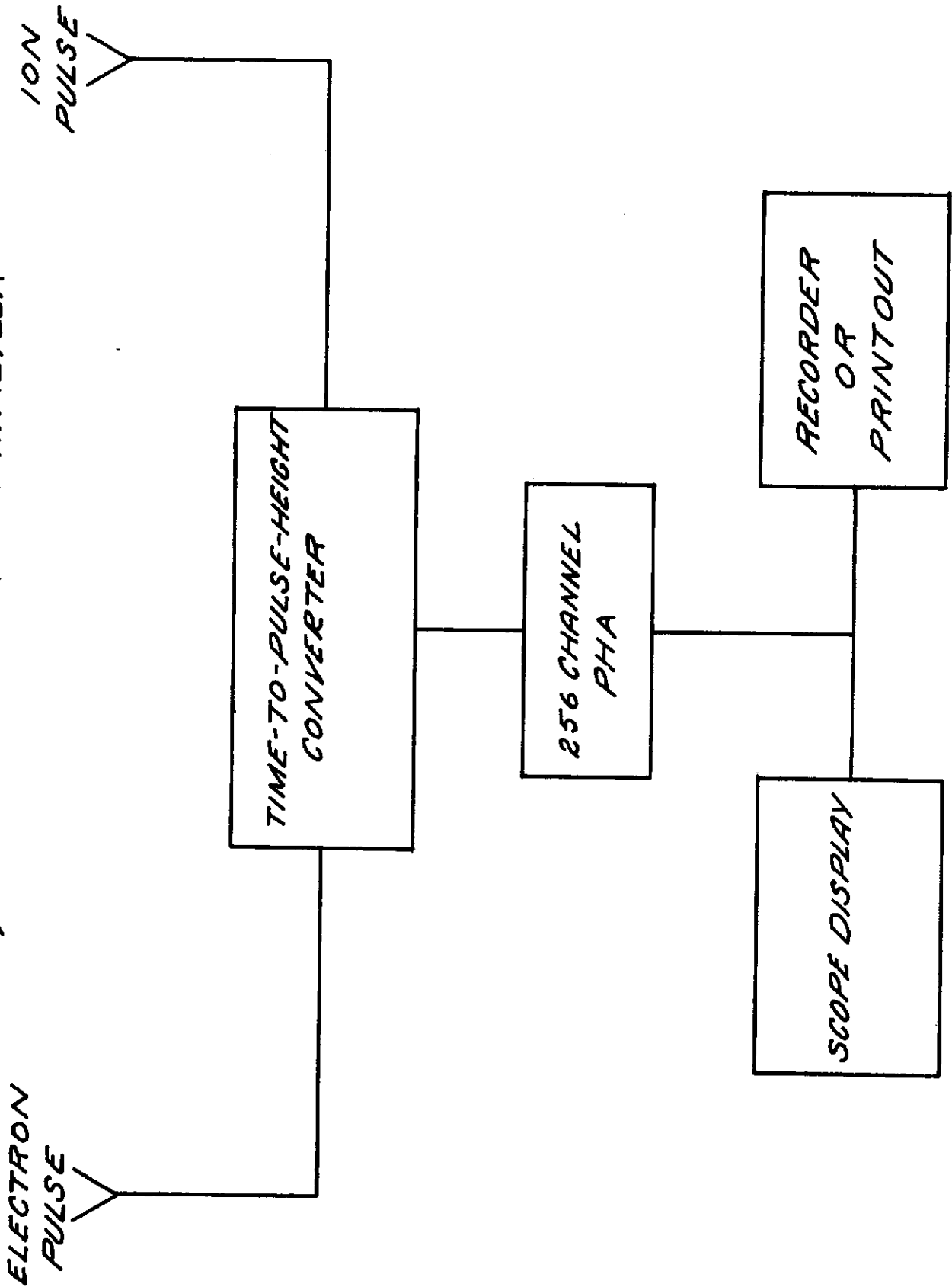


Figure 4 Block diagram of data handling system using multi-channel pulse height

In addition, any mass range can be selected and investigated separately by expanding the time scale and selecting the time interval of interest. Small time intervals, in other words small windows, mean reduction of the background; large expansion gives improvement in resolution.

### III. THEORETICAL CONSIDERATIONS

#### A. FUNDAMENTAL RESEARCH NEEDS IN RADIATION EFFECTS ON MATERIALS

To a very large extent, the critical effects of radiation on materials of present scientific and technological importance depend upon the chemistry that is induced by the impingement of radiation. Any program concerned with radiation effects, must, therefore, be a rational attempt to understand this exceedingly complex chemistry.

The primary act involved in the passage of radiation through a chemical system is the production of ionization and excitation, viz.



The asterisk on the ionic species  $M_1^{+*}$  indicates that the ion need not be in its ground electronic state. Although the production of one ion-pair, as in Reaction (2), requires on the average the expenditure of 30 electron volts, the details concerning the relative distribution of energized and ionized species constitute a major problem in the physics of the primary process. Studies of the energy spectrum of the secondary electrons formed in (2) can lead to, at the least, a partial knowledge of the excitation distribution in the ionic species, and, therefore, constitute an important part of the complete solution of the problem of the primary radiation chemical act. Radiation chemistry, which comprises the sum total of all reactions of the energized and ionized species formed in the primary act, may be said to begin subsequent to the occurrence of Reactions (1) and (2). Fundamental research needs can thus be discussed in terms of the primary radiation chemical act described above and the possible reactions of  $M_1^*$  and  $M_1^{+*}$  described below.

#### 1. Unimolecular Dissociation

These reactions may be summarized as follows:



Much valuable information concerning (3a) and (3b) is already available in the literature from studies of thermal and photochemical decompositions.

The ionic species  $M_1^{+*}$  can dissociate also, and in this case there results a set of primary ionic species,  $P_i^+$ , and corresponding neutral fragments,  $N_i$ , which may be free radicals or stable molecular products. The obvious source of valuable knowledge of Reaction (4) is from studies of the mass spectra.

Such spectra, however, as measured in a mass spectrometer, represent ionic distributions  $10^{-6}$  seconds after the primary act, while collision times in radiolysis are  $10^{-10}$  seconds or less after the primary ionization act. Moreover, usual mass spectra are derived from the impact of 50 - 70 electron-volt electrons which may lead to significantly different ionic distributions than are encountered in radiolysis. The significant differences are probably due to the distribution of excitation in the primary ion  $M_1^{+*}$ . It is precisely this excitation energy distribution which is needed in calculations of the mass spectral time dependence and hence in ionic distributions at  $10^{-10}$  seconds.

The complications as outlined above make it imperative, for an understanding of the influence of Reaction (4) or radiolysis effects, that fundamental information be obtained on the following:

- (1) The energy spectra of the ions and secondary electrons formed in the ionization act.
- (2) The effect of energy and radiation type on the mass spectra of simple molecules.
- (3) Theoretical studies of the time dependence of the mass spectra of simple molecules.

## 2. Bimolecular Reactions Involving $M_1$

These reactions may be summarized as follows:



The excited species  $M_1^*$  can be deactivated by collision to states of lower excitation,  $M_1^t$  and  $M_1''$ , and such processes are continued until the initial excitation energy is degraded. Examples of chemical change occurring in the collision are not well-documented, and so, while we admit their possibility, we ignore them in this discussion. The ionic species,  $M_1^{+*}$  and  $P_i^+$ , can react with  $M_1$  on collision in what are now commonly called ion molecule reactions. In Reactions (6) and (7) the symbol,  $S^+$ , denotes secondary ions. Much-needed kinetic information concerning such reactions is obtainable from studies of the pressure dependence of mass spectra. Of particular value would be studies of the pressure dependence of mass spectra derived from the impingement of high energy electromagnetic radiation.

The free radical  $R_i$  can react upon collision with  $M_1$  to form product molecules  $M_4$  and another free radical  $R_j$  or simply a new free radical  $R_k$ . A large body of information, mostly derived from photochemical and thermal studies, is available concerning such reactions

### 3. Neutralization of Ions.

In studies of ion-molecule reactions in a mass spectrometer, a neutralization of ions need not be considered but definitely must be in studies of radiation effects on materials. Indeed, for a given dose rate, the lifetime of the various ionic species will be determined by the specific reaction rates of ion-molecule reactions and ion-neutralization reactions. As this may be reflected in the observed physical and chemical changes, much research on the neutralization process in radiation chemistry is needed.

There is available a large amount of data consisting of product analyses of irradiated chemical systems. However, it is fair to state that an understanding of radiation effects will only come about through independent studies of the elementary processes that make-up the overall process. It is in studies of the physics and chemistry of these elementary processes that our research needs are the greatest and in which our research efforts will be the most fruitful.

### B. IONIZATION OF MOLECULES BY X-RADIATION

A number of photon impact studies of molecules using a mass spectrometer have been reported (1, 2, 3, 4) using radiation in the vacuum ultraviolet region. The photon energies which have been used are in the 7-15 ev range. These studies have resulted in rather precise measurements of outer shell ionization potentials and have given detailed information concerning the fragmentation patterns of polyatomic molecules at energies near the ionization potential.

The present x-ray photo-impact studies of polyatomic molecules using the coincidence mass spectrometer were aimed at a better understanding of inner shell ionization processes and of the rearrangements and dissociations which follow. In this work, x-ray photons in the relatively "soft" (1000-6000 ev) range were used.

When a soft x-ray photon interacts with a bound electron of an atom or molecule, by far the most probable process which can occur is the photoelectric ejection of an electron. In particular, if the photon is sufficiently energetic, the electron will most probably be ejected from the inner or K-shell. This interaction results in the formation of a very highly excited ion since the low-lying K-shell now lacks an electron.

In a very short time ( $\sim 10^{-10}$  sec.) the ion loses its excitation by an outer shell electron dropping down into the unfilled K-shell. When this occurs the excess energy is emitted either in the form of a fluorescent x-ray or by the Auger effect.

For the lighter elements eg carbon, with which we are concerned in the study of hydrocarbon molecules, the Auger effect is the most probable. In the Auger effect the excess energy is carried away by one or more outer shell electrons being ejected, with their total kinetic energy plus their binding energy being equal to the energy of the fluorescent x-ray which otherwise would have been emitted.

Thus it is expected that, when molecules of a hydrocarbon gas are ionized by x-ray photon impact, a very large fraction of the ions produced will be multiply charged. Since multiply charged hydrocarbon ions tend to be unstable, the probability of very rapid dissociation is quite large. For these reasons it is expected that the degree of fragmentation will be larger when ionization is due to x-ray photon impact rather than to an equivalent electron impact.

When dense samples of a material (even a gas at atmospheric pressure) are irradiated with x-rays the primary interactions of the x-ray with the atomic electron is obscured by the action of the secondary electrons. Since the cross section for ionization by electrons is many orders of magnitude larger than for ionization by x-rays of the same energy, most of the ionization, and, hence, most of the chemical changes produced in an irradiation of a dense sample with x-rays, are caused by the secondary electrons. Thus irradiation experiments of this kind give very little information concerning the primary interaction of the x-ray photon with the primary atom or molecule.

The experimental difficulties which have prevented the previous direct measurement in the conventional mass spectrometer of the fragmentation patterns of hydrocarbon molecules due to ionization by x-rays include the following:

- (1) The cross section for ionization by x-rays decreases as  $1/E^4$  as the energy,  $E$ , of the x-ray increases.
- (2) The intensity available from an x-ray tube decreases as the energy of the x-ray decreases due to the rapid increase of the absorption coefficient in window materials with decrease in energy.

These factors make the production of sufficient ion intensity to be measurable above random background noise by conventional mass spectrometry extremely difficult or impractical. The coincidence mass spectrometer has a sufficient sensitivity to overcome this obstacle.

By use of the coincidence principle, the ion counting circuit is turned on for only a few microseconds after a secondary electron has been detected. Thus, at a counting rate of one ion per second, the ion detector is sensitive for only about 10 microseconds out of each second of operation. The ratio of sensitive time to dead time for random background signals is thus about  $10^{-5}$  at this counting rate, while this ratio for the desired ions is essentially unity. This is the primary feature of the coincidence mass spectrometer which makes the measurement of x-ray induced ionization and fragmentation feasible.

## C. ION OPTICS

To make sure that the highest energy secondary electrons will impinge on the first dynode of the electron detector, the voltages of the separation grids must be sufficiently high (5000 volts). The positive ions in turn are accelerated in the opposite direction. Their time-of-flight is given by

# Contrails

$$\tau = \frac{\sqrt{2ma}}{\sqrt{qE_1}} \left( 1 + \beta \sqrt{\beta^2 + \frac{s}{a}} - \beta^2 + \frac{\beta d}{2a \sqrt{\beta^2 + \frac{s}{a}}} \right) \quad (3)$$

where

m = mass number

a = half distance between grids no. 1 and no. 2

s = distance no. 2 and no. 3

d = length of drift tube

E<sub>1</sub> = electric field in region I

E<sub>2</sub> = electric field in region II

$\beta^2 = E_1/E_2$

q = charge

Taking the appropriate values for the parameter in the above equation,  $\tau$  is essentially determined by the last expression in the bracket. In other words, the time spent in the acceleration regions is negligible compared to the drift time. If the electrical fields are replaced by the voltages  $U_1 = aE_1$  and  $U_2 = sE_2$ , the number of parameters is reduced to three, excluding m and q. Two parameters may be chosen according to considerations which are mentioned below. The third parameter  $\beta$  is then determined by the Wiley (5) condition for space resolution.

$$d = 2ak^{3/2} \left( 1 - \frac{1}{k + k^{1/2}} - \frac{s}{a} \right) \quad (4)$$

where

$$k = 1 + \frac{d}{a} \beta^{-2}$$

In the case of ionizing under x-ray bombardment one has to make sure that the highest energy secondary electrons will impinge on the first dynode of the electron detector. The x-rays used correspond to an energy up to 5000 volts. Thus, one can expect a number of secondary electrons which have energy slightly below 5000V. To deflect those electrons into the detector, at least 5000 volts across the ionization region are necessary;  $U_1$  is then determined. The transit time  $\tau$  for a given mass m is chosen in such a way that the time scale is compatible with the resolution of the electronic circuits and the dimensions of the spectrometer.

The choice of these parameters are listed in Fig. 5. It should be pointed out that the absolute value of these voltages can be varied without changing the resolution provided that the ratio  $E_1/E_2$  remains constant. In general, low voltages produce long transit times.

Any initial energy distribution of the ions will not influence the overall resolution provided the voltages across the first region is sufficiently high. The time-to-mass correlation of equation (3) indicates that the maximum resolvable mass is around mass 80 and is determined by the succeeding electronic circuitry, particularly, by the frequency response of the electron

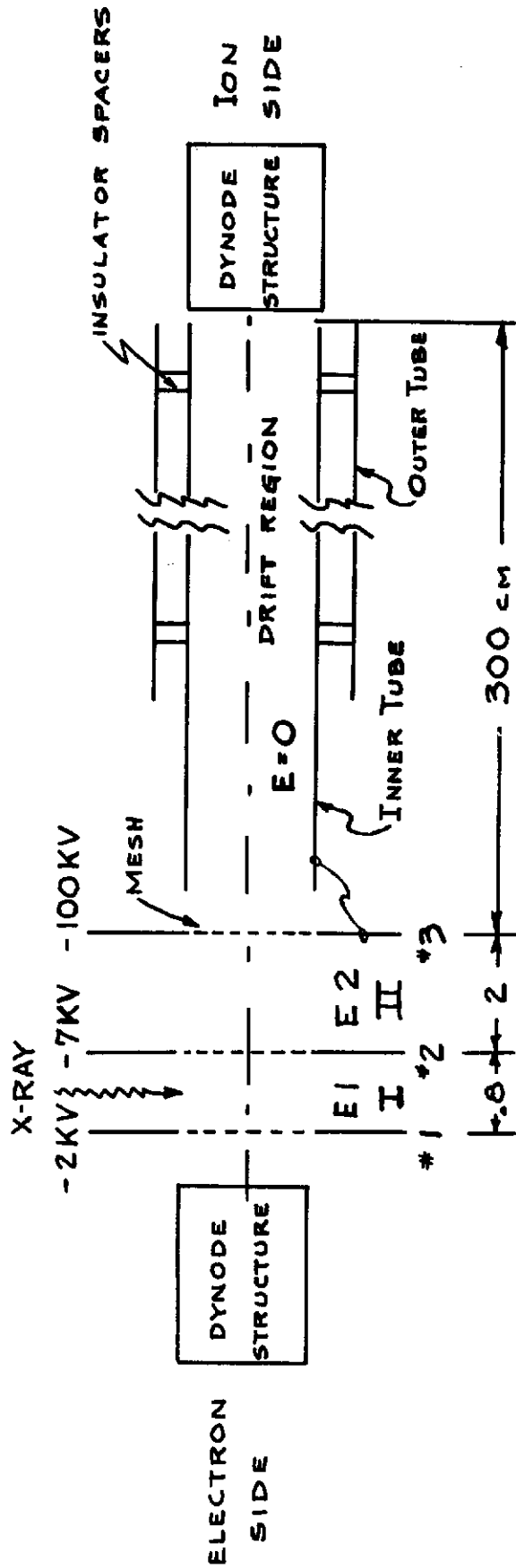


Figure 5 Grid Structure With Voltages For Desired Ion Optics



multiplier tubes and the subsequent pre-amplifiers. The calculated space resolution from Equation (4) is much better.

## IV. DESIGN MODIFICATIONS AND CONSTRUCTION OF EXPERIMENTAL SYSTEMS

### A. INTRODUCTION

The experimental system consists chiefly of the source of radiation, the ionization chamber and grid structures, the ion drift tube, the electron and ion detectors, the pumping and sample systems, the data handling systems, and the associated electronics. These components, many of which are special in design, are described in the following sections.

This system was constructed of stainless steel for mechanical strength, chemical inertness, and freedom from magnetic fields. Provisions were made for easy assembly and exchange of essential parts. By the use of high-vacuum tight flanges the various parts of the system are separately detachable. The considerable number of flanges which were required made it advisable to rely on a dependable and flexible type of flange and gasket. It was decided, therefore, to use complementary step flanges with gaskets of hydrogen-annealed copper rings. The complexity of the spectrometer and the tight specifications concerning alignment, tolerances, and insulation required considerable effort in the machining work. An overall view of the system is shown in Figure 6.

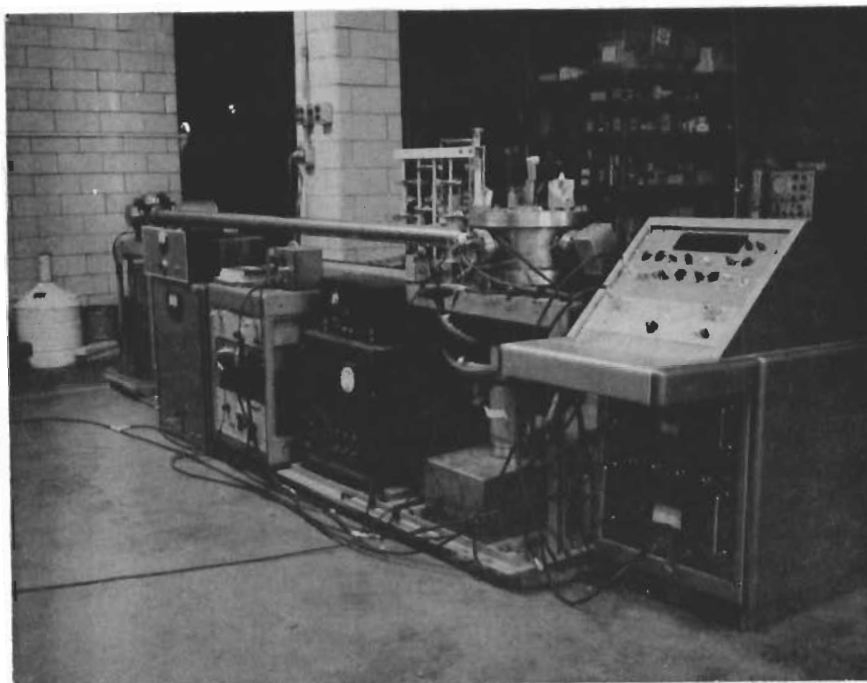


Figure 6 Overall View of Experimental System.

## B. SPECIAL X-RAY TUBE

The special x-ray tube developed for studying the inner shell ionization of molecules by x-rays has been described in Part I. This x-ray tube was required, in addition to the extremely high sensitivity of the coincidence mass spectrometer, to surmount the principle obstacle to these studies posed by the extremely small cross-sections for x-ray ionization as compared to the cross-sections for ionization by electrons. An x-ray tube meeting these requirements was not available commercially. Therefore, a completely new x-ray tube was designed and constructed.

This special x-ray tube incorporates the following unique features:

### 1. Long wavelength cut-off

The tube uses a very thin beryllium window together with an aluminum target. This results in an x-ray spectrum dominated by the aluminum K $\alpha$  line at 8.32 A with approximately a 10 A window cut-off. This may be compared with the lowest energy x-ray tube commercially available which uses an iron target for which the K $\alpha$  line is at 1.93 A and which has a window cut-off at about 2 A.

### 2. Beam definition

The aluminum target and electron gun in the x-ray tube were specially designed to give a rectangular x-ray beam less than 2 mm. wide at 10 cm from the target. The narrow, well-defined x-ray beam is required to obtain usable resolution in the mass spectrometer. This improved focus of the electron beam, which is better than that of any known x-ray tube, is made possible by a single wire filament which runs at low voltage (1.5 volts) and at high current (30 amperes.)

### 3. Demountable

The x-ray tube is easily demounted from the ionization chamber for repairs, adjustments, or substitution of a different target. The vacuum system is completely independent of other components and consists of a small titanium ion pump. The beryllium window easily withstands exposure to atmospheric pressure for long periods with the x-ray tube evacuated.

This special x-ray tube has been successfully built and tested. It has been used in this research as an integral part of a modified Coincidence Mass Spectrometer performing basic studies on x-ray ionization and fragmentation of molecules.

## C. THE IONIZATION CHAMBER

The ionization chamber consisted of a stainless steel cylinder, 15 inches

in diameter and 9 inches high, with removable top and bottom plates and 5 side ports. A photograph of this unit is shown in Figure 7. Top and side views are represented schematically in Figures 8 and 9 respectively. A sectional view is shown in Figure 10.

The large size of this chamber was desirable to provide unobstructed mounting for various devices which must be arranged around the ionization region. The most important of these are the complex grid structures, which are shown schematically in Figure 9.

Three slits were located on top of the x-ray port to obtain a well-defined beam; and also to extract and separate the electrons and ions formed by the x-ray beam outside of the primary ionization region. This region was defined by two plates, each 3.5 inches square. Additional plates were provided to re-accelerate and to focus the desired ions and electrons. Field penetration through the holes was prevented by the use of fine nickel mesh of 90 per cent transparency. All structures inside the ionization chamber were most carefully aligned with both the x-ray beam and the centerline of the drift tube. These alignments were necessary to prevent loss of ions by wall collision in the drift tube, or loss of resolution by uncertainty of the geometric location of ionization in the chamber.

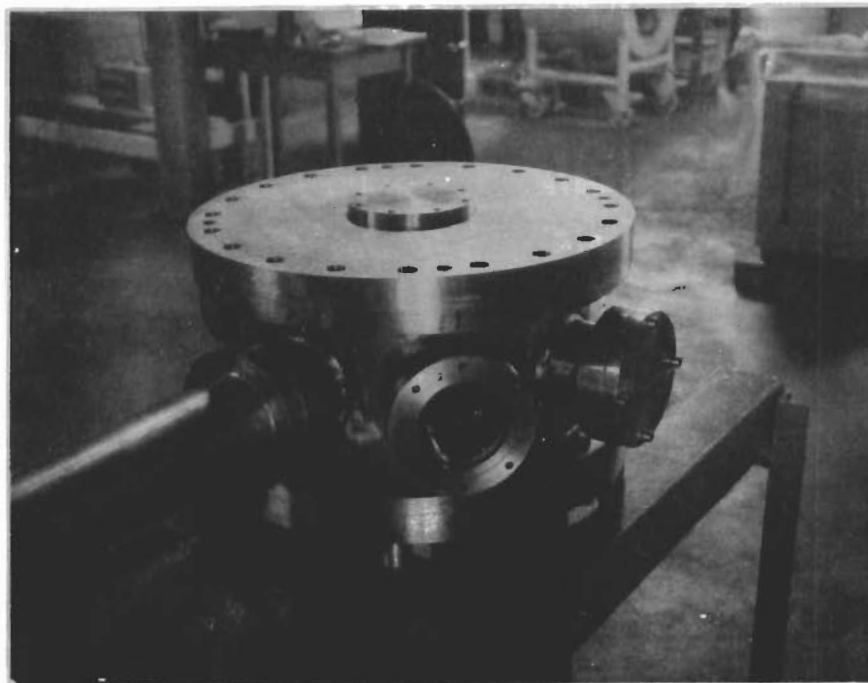


Figure 7 Ionization Chamber Showing, Left to Right, Ion Drift Tube, Electrical Feedthrough Port, and Access Port to Electron Gun.

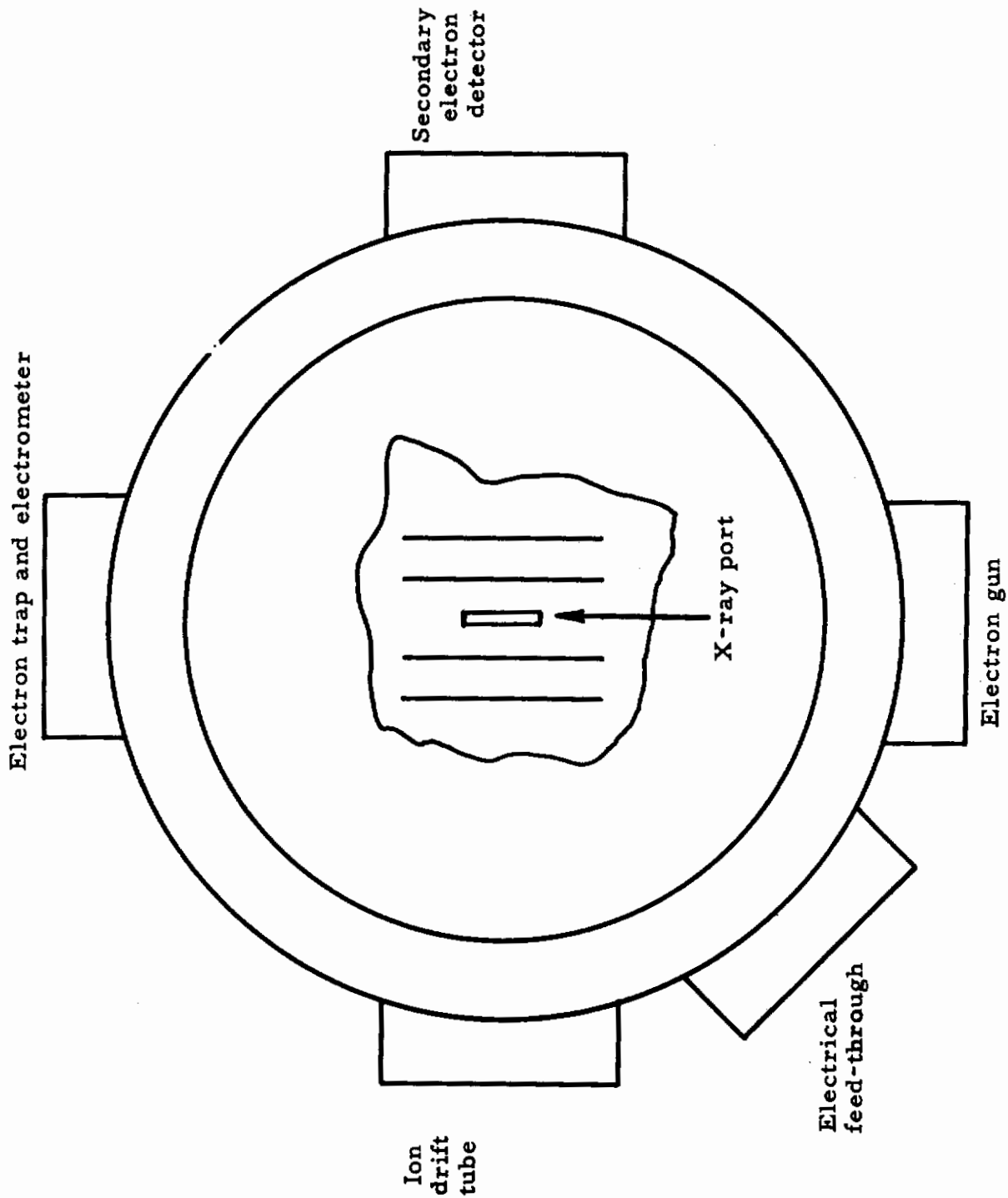


Figure 8 Schematic Drawing of Ionization Chamber, Top View

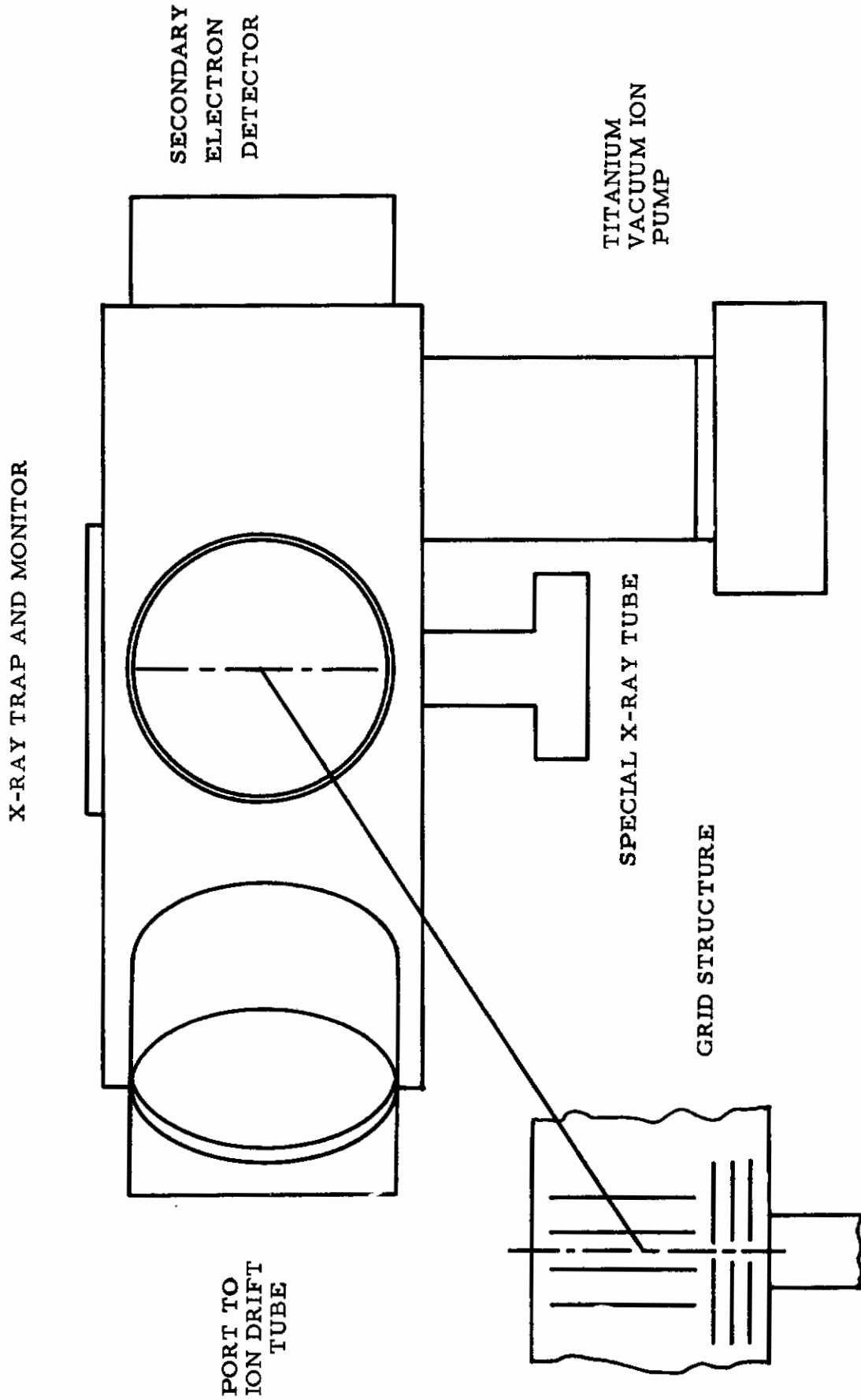


Figure 9 SCHEMATIC DRAWING OF IONIZATION CHAMBER, SIDE VIEW

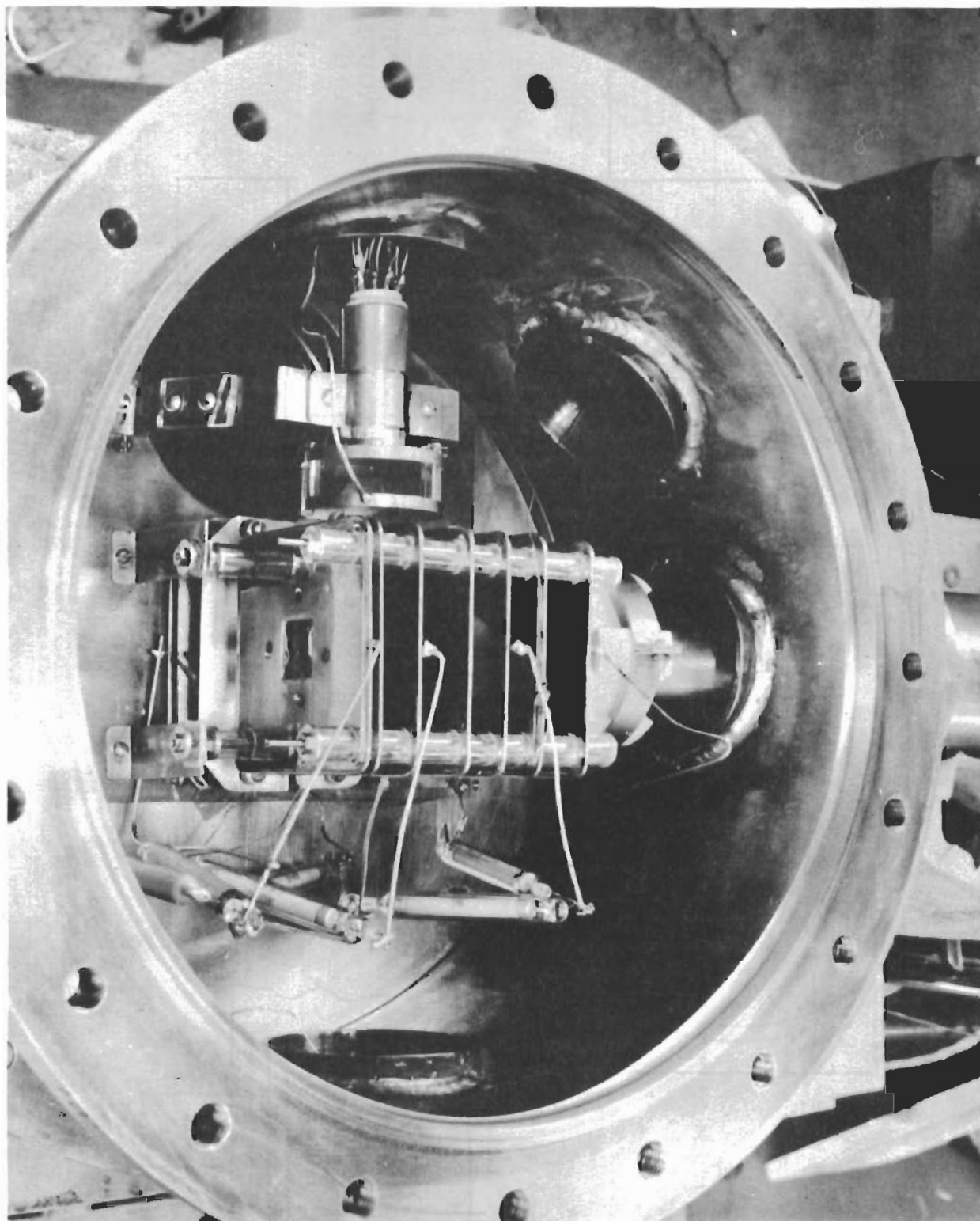


Figure 10 Top view of inside of ionization Chamber.

For the calibrations and the electron studies an electron gun was also incorporated in the ionization chamber. A National Union Model 1-DP commercial electron gun was used for this purpose. This gun gives a nominal 1 mm. cylindrical beam at an energy of 600 electron volts. A reaccelerator region was provided in front of this gun to obtain higher energy electrons when desired. This gun was faced by an electron trap for monitoring the electron current with a sensitive electrometer.

## D. THE GRID STRUCTURES

The grid structures, a vital part of the instrument, are shown schematically in Figure 9. These structures enclose the ionization area in which the ions and their corresponding electrons are produced. They are shown photographically in Figures 11 and 12.

Each grid plate was constructed of two pieces of .031 stainless steel spot-welded together with a 50 lines per inch Buckbee-Mears etched mesh in between. This mesh stretched across the apertures in the plates through which the ion and secondary electron beams pass. These plates were clamped together with four stainless steel screws. The spacing between grid plates and electrical insulator was provided by precision-ground pyrex glass spacer.

It is imperative that the plates be aligned with the drift tube and with the x-ray tube. The tolerances of these alignments were calculated as follows:

The maximum angle tolerance between the center lines of the drift tube and the grid structures is very nearly

$$\Phi = \frac{\Delta S}{D} \quad (5)$$

where  $\Phi$  is the angle between the center lines of the grid structures and drift tubes,  $D$  is the distance between the ion detector and the point of intersection of the center lines, and  $\Delta S$  is the radial deviation of the ion from the drift tube center line at the ion collector.

If, for example,  $D$  is 300 cm. and the angle is 5 seconds, the impact point of an ion on the target will be off center by  $\Delta S = 0.4$  cm.

The travel time of an ion is approximately

$$\tau_x = 1.02\sqrt{m} \left( \frac{a}{\sqrt{U_1}} + \frac{D}{2\sqrt{U_1+U_2}} \right) \quad (6)$$

Notations are the same as on page 13.

During the time  $\tau_x$ , the ion reaches the point  $(x, y)$  where  $x$  is the coordinate axis coincident with the center line of the drift tube and  $y$  is the coordinate axis radial to this center line.

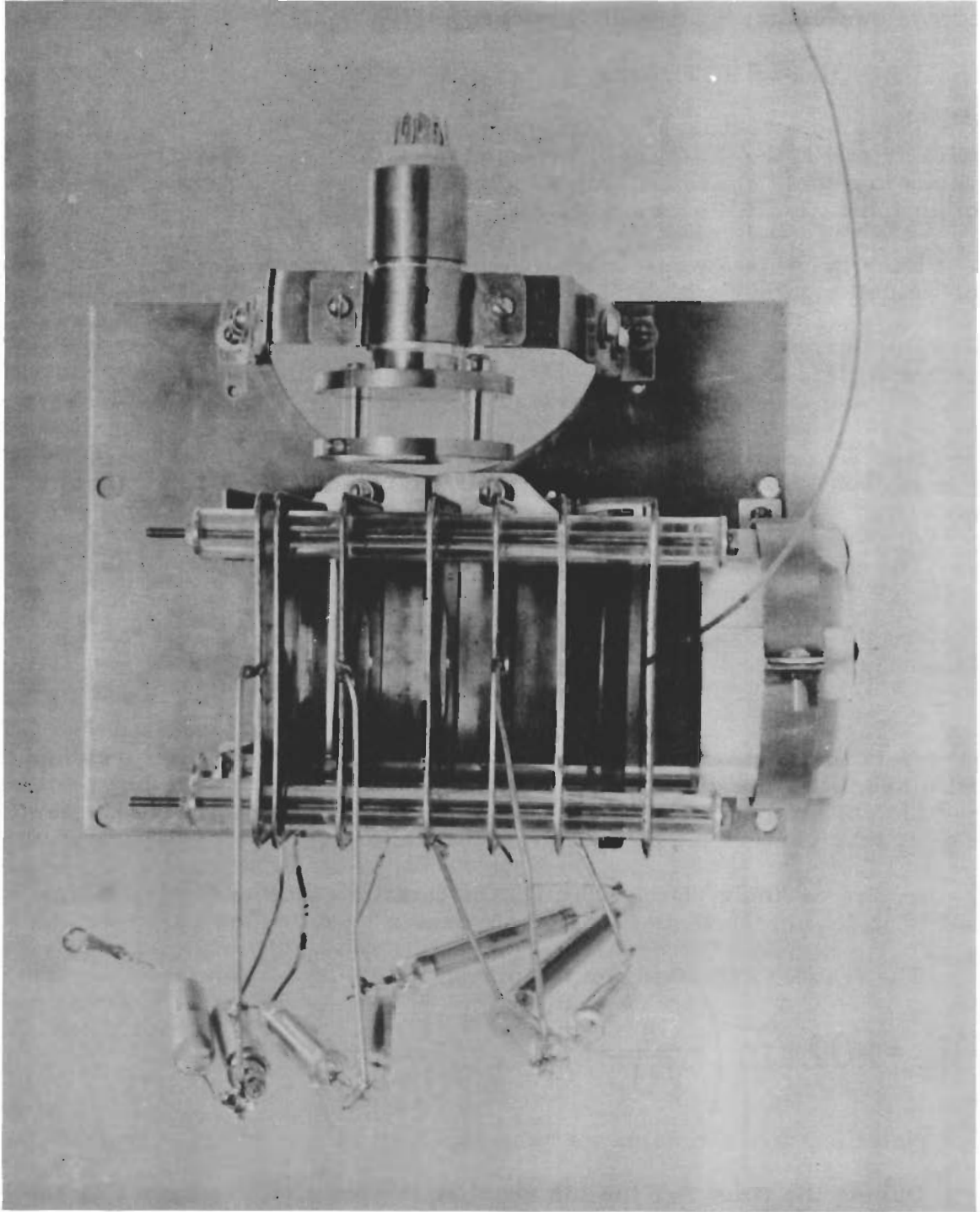


Figure 11 Grid Structures, Top View.



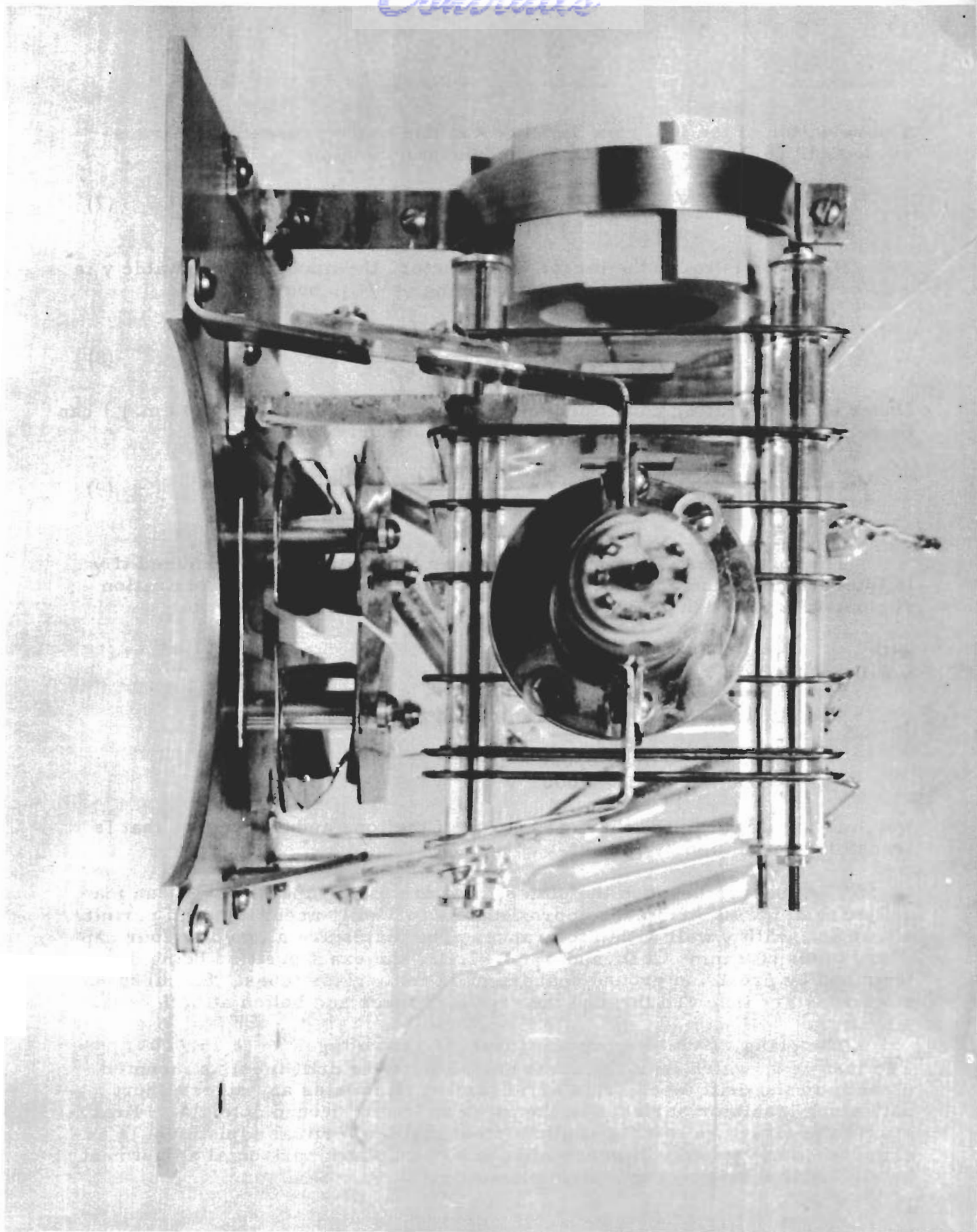


Figure 12 Grid Structures, Side View.

# Contrails

The deviation of the ion from the x-axis is due to the presence of a transverse field component,  $U/y$ , in the acceleration region.

$$Y = \tau_x \frac{2\sqrt{U}}{\sqrt{m}} \quad (7)$$

If the ion is to hit the target, or detector, the maximum allowable  $y$  is  $\pm 2.0$  cm., thus determining  $U$ . Introducing  $\gamma = U/U_1$ , one obtains

$$1 + \frac{D/a}{2\sqrt{\frac{U_1+U_2}{U_1}}} = \frac{Y/a}{2\sqrt{\gamma}} \quad (8)$$

Under usual operating conditions and geometry ( $D = 300$  cm.,  $a = 6$  cm.) 1 can be neglected on the left-hand-side with little error. Hence,

$$\gamma \leq \frac{U_1+U_2}{U_1} \times \frac{Y^2}{D^2} \quad \gamma \leq \frac{U_1+U_2}{U_1} \times 4.45 \times 10^{-5} \quad (9)$$

The tolerances of the spacers between the plates are determined if  $\gamma$  is interpreted as the angle between the two plates bordering the ionization region, which in turn causes the transverse field component.

with  $U_1 = 10,000$  V,  $U_2 = 7U_1$   
 $\gamma$  will be  $\gamma = 3.56 \times 10^{-4}$  or 1.5 sec.

The allowable value of the transverse component is

$$U = 3.56 \text{ V at } U_1 = 10,000 \text{ V and} \\ U = 356 \text{ mV at } U_1 = 1000 \text{ V}$$

which is greater than the thermal energy of the ions and any energy that is transferred to an ion by impact.

The spacers between the plates, that are 6 cm apart, have been machined to  $2.1 \times 10^{-3}$  cm, or approximately to 1 mil accuracy, and permit alignment, with  $\gamma$  well within tolerance. The plates are aligned on four capillary tubes of 9 mm O.D. and 3 mm I.D., the exact position being determined by precision ground spacers of 12 mm glass tubes. Stainless steel rods are inserted through the capillary tubes and bolted at both ends.

The glass insulators provide insulation to voltages up to 15,000V. The last grid, which is at the same potential as the drift tube, is mounted directly to the drift tube. This arrangement eliminates any direct short path along insulator surfaces to the parts at low or ground potential. Brackets tie the structure to a flat-bottom steel plate. Vertical adjustment is accomplished by two sets of screws in the bottom plate; horizontal adjustment by sliding brackets on the bottom plate.

To obtain a well defined beam and to extract the extraneous electrons and ions generated in the region between the x-ray port and the ionization chamber, three slits are located horizontally on the top of the x-ray port beneath the ionization region.

The electron gun is enclosed in a tight fitting cylinder. A one mm hole in the disc at one end of the cylinder defines the cross-section of the electron beam; a second disc in front of the gun allows additional acceleration of the electrons. This device is insulated from the bottom plate and is adjustable with respect to the ionization region.

## E. THE DRIFT TUBE AND ION DETECTOR

The drift tube actually consists of two concentric stainless steel pipes. The minimum diameter of the inside tube is determined by the useful area of the ion detector. The outer tube is 3 inches in diameter. Pyroceram spacer rings with narrow tolerances in their dimensions hold the inner tube in position and provide safe electrical insulation. The walls of both tubes which face each other are polished to avoid field emission.

The physical arrangement of the ion drift tube in relationship to the ionization chamber is shown in Figure 13. The modified support structure for holding this system is clearly shown.

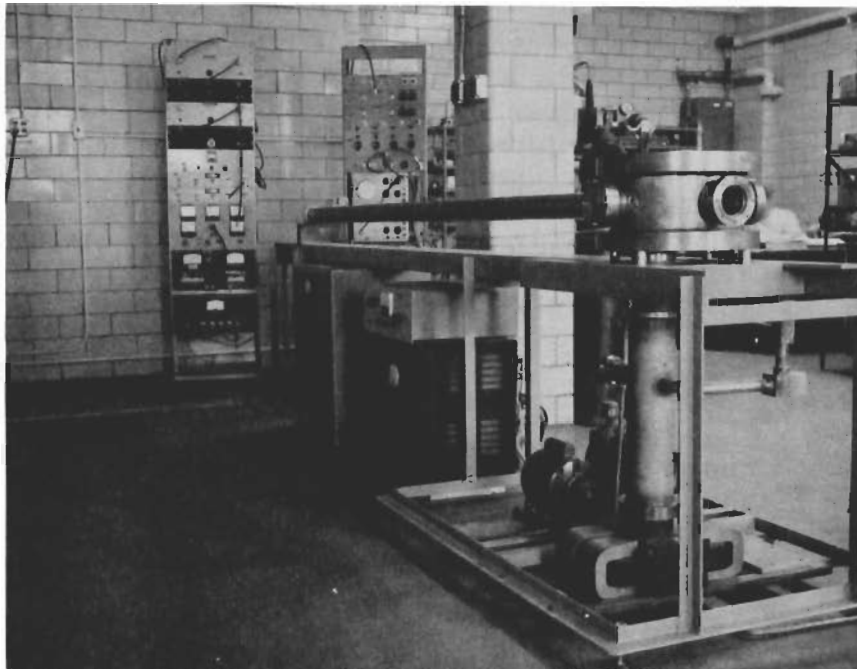


Figure 13 Photograph Showing Drift Tube, Ionization Chamber, and Pumping System of Coincidence Mass Spectrometer.

The detection of the ion necessitates an elaborate device, considering the fact that the ions have a high kinetic energy (6). The approach is briefly described as follows. The ion impinges on a polished aluminum plate releasing secondary electrons from the surface. The electrons, (on the average 10 electrons per ion), are deflected to a disc of plastic scintillator which is protected by a thin metal window. The resulting scintillation is detected by a photomultiplier tube, thus producing a voltage pulse. The complexity of the ion detector device and the necessity of using differential pumping required the construction of a vacuum can of the same principal design as the ionization chamber, but much smaller and simpler. A special high voltage feed-through connector is mounted on one of the four existing ports of this can.

## F. THE PUMPING SYSTEM AND SAMPLE HANDLING SYSTEM

The use of titanium vacuum ion pumps simplifies the entire vacuum system considerably. Thus, liquid nitrogen cold traps, vacuum gauges, and valves are eliminated or reduced to a minimum. One single forepump works as a roughing pump and operates the sample handling system.

Two separate titanium vacuum ion pumps are used, one for the main chamber and one for the differential pumping of the can at the end of the drift tube. This arrangement insures that the pressure inside the drift tube will be lower than in the ionization chamber by about one order of magnitude. This is important to minimize the number of collisions between the drifting ions and gas molecules.

The sample gas under investigation is placed in a reservoir flask following simple purification by a cold trap. The gas is then allowed to flow through a 0.005 in. diameter capillary about 3 feet long, and is injected directly above the ionization region. The pressure is measured by an ionization gauge near the ionization chamber. An alternate method is also provided. The pressure in the reservoir is accurately and absolutely determined by a Dubrovin gauge. Knowing the pressure drop in the capillary, the actual pressure at the end of the capillary, and thus in the ionization region, is calculated. Photographs of the pumping system and the sample handling system are shown in Figures 14 and 15, respectively.

## G. TIME ANALYZER AND RELATED CIRCUITS

The most important system of the electron circuitry is certainly the time-to-pulse height converter and multi-channel pulse height analyzer. Many approaches to time conversion were investigated. Three circuits were emphasized.

In the first method both the electron and ion signals generate a rectangular pulse each of definite length and the same or opposite polarity. The overlapping part is integrated and the resulting pulse, which is approximately triangular, is analyzed in the memory core pulse height analyzer. One major disadvantage of this approach is the change of pulse length with the change of amplitude. Shaping of the pulses without losing the pulse height information establishes a fairly difficult problem.



Figure 14 Pumping System

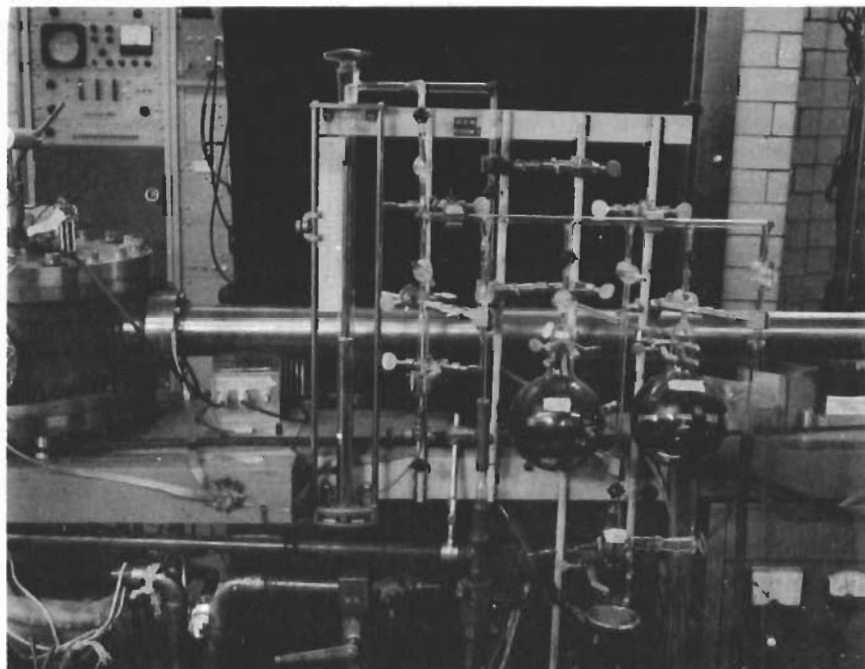


Figure 15 Sample Handling System.

# Contrails

In the second method the electron pulse generates a sawtooth which is cut or clamped at the very moment an ion pulse arrives. If the sawtooth is clamped, the base length of the pulses is independent of the pulse height. Furthermore, no problem is involved in obtaining output pulses of identical waveform by cutting off the first (ramp) part of the pulse in a gate circuit.

The third method involves a very elegant and appealing method first suggested by Waters (7) which avoids the double conversion from time-to-pulse height and pulse-height-to-time, the latter being done by the pulse height analyzer. In principle, the delay time between the arrival of an electron and ion is counted by a train of pulses supplied from a crystal-stabilized oscillator. The pulses are fed directly into the address scaler of the memory core. The standard address scalers are, however, unable to accept pulses shorter than 0.5 microseconds. That makes them useless for measuring short time intervals. If a fast scaler is used, however, to count a train of 10 nanosecond pulses and the address scaler to count the complement to a predetermined number, i. e. 200, using subsequent 2 megacycle pulses, the resolution can be considerably improved, in this particular case to almost 10 nanoseconds.

A number of test circuits have been developed based upon these principles. However, reliability, testing time, and costs had to be considered. Thus the second method was emphasized in our work.

In this approach the electron pulse triggers a flip-flop gate, which in turn, triggers an adjustable sawtooth of 1 to 4 microseconds in length after a present delay time variable in the range from zero to 12 microseconds. Each ion pulse, shaped in a flip-flop, is fed into a gate and holding circuit together with the sawtooth. The sawtooth is clamped whenever the ion pulse arrives during the duration of the sawtooth. The tail of the sawtooth starts a rectangular pulse of 20 microseconds in length. This pulse has two functions: firstly, to cut off the output pulse of the holding circuit, so that all pulses have the same length and secondly, to reset the flip-flops and thus determine the dead time of the entire circuit. After appropriate amplification, the pulses are analyzed and displayed in the 256 channel memory core analyzer. Also provision has been made to adjust all pulses to constant length and shape by adding a univibrator and an additional gate.

Making use of the latter circuit the whole spectrum can be analyzed in one single operation. In this case, the resolution is calculated to be 60 nanoseconds taking a maximum drift time of 15 microseconds and breaking it into 250 channels. In designing this device, special attention has been given to the hold-on circuit. The tests of an experimental setup have given an excellent result. This approach is shown schematically in Figures 16 and 17. It was used in the present investigations.

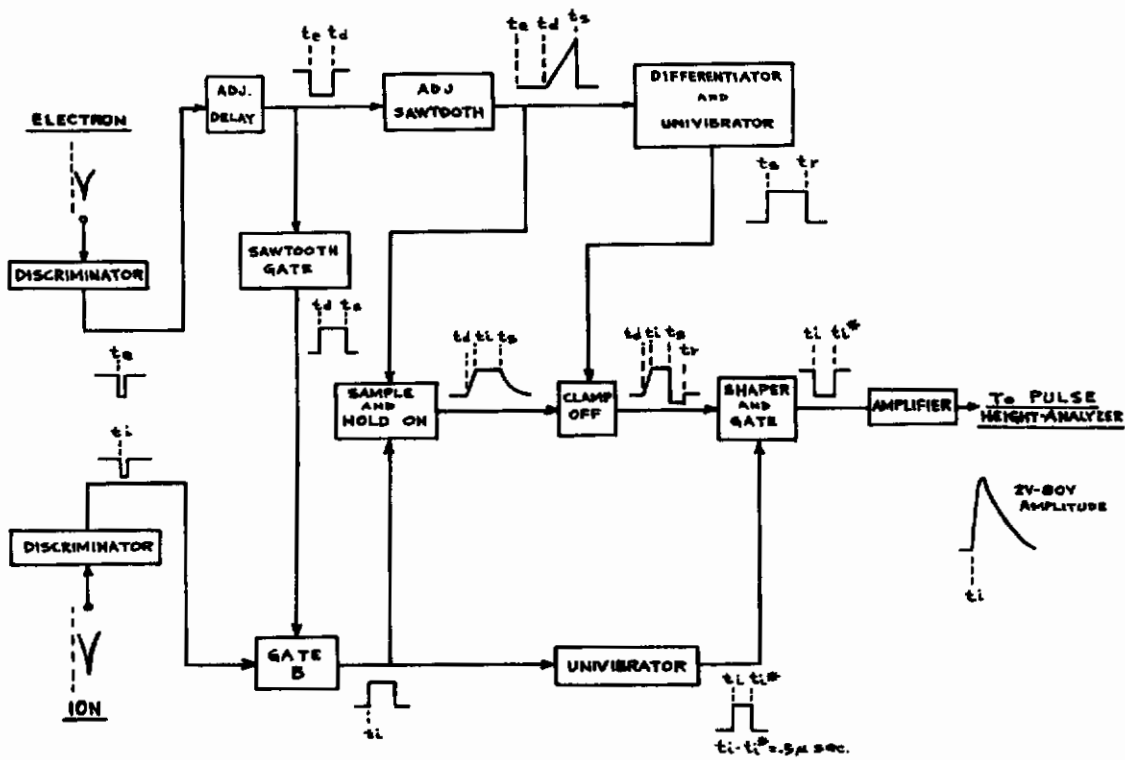


Figure 16 Block Diagram of Time-to-Pulse-Height Converter.

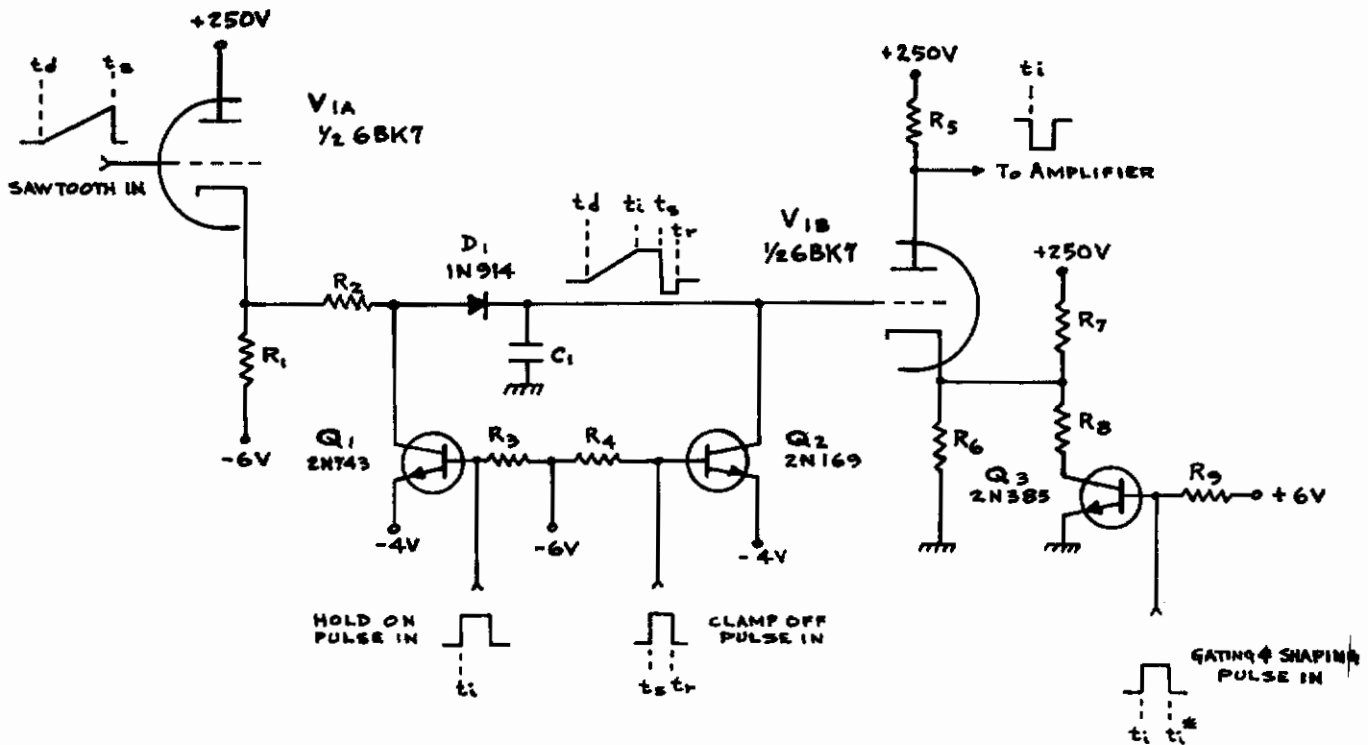


Figure 17 Section of Time-to-Pulse-Height Converter Showing Slightly Simplified Circuit Diagram of the Hold-on and Gate Circuit.

## V. RESULTS AND DISCUSSIONS

### A. CALIBRATIONS

The first calibrations were the tests on the vacuum in the ionization chamber and drift tube. After repeated leakage checks and baking-out procedures, the system showed a final vacuum of better than  $10^{-6}$  mm. Hg. However, the titanium Vac-Ion-Pumps used in the system have the property of releasing previously pumped atmospheric argon in this pressure range; this is manifested by cyclical fluctuations of the pressure between  $4 \times 10^{-7}$  and  $4 \times 10^{-6}$  mm. Hg.

In operation, the pressure of the gas sample was determined in several ways. The most accurate method was reading the pressure in the sample handling system from the Dubrovin Gauge and calculating the pressure in the ionization region by the use of Knudsen's Law for molecular gas flow through a capillary tube. The experimental calibration of two different gases is shown in Figure 18. The experimental calibration for nitrous oxide coincides with the theoretical calculation which is indicated by the dotted line.

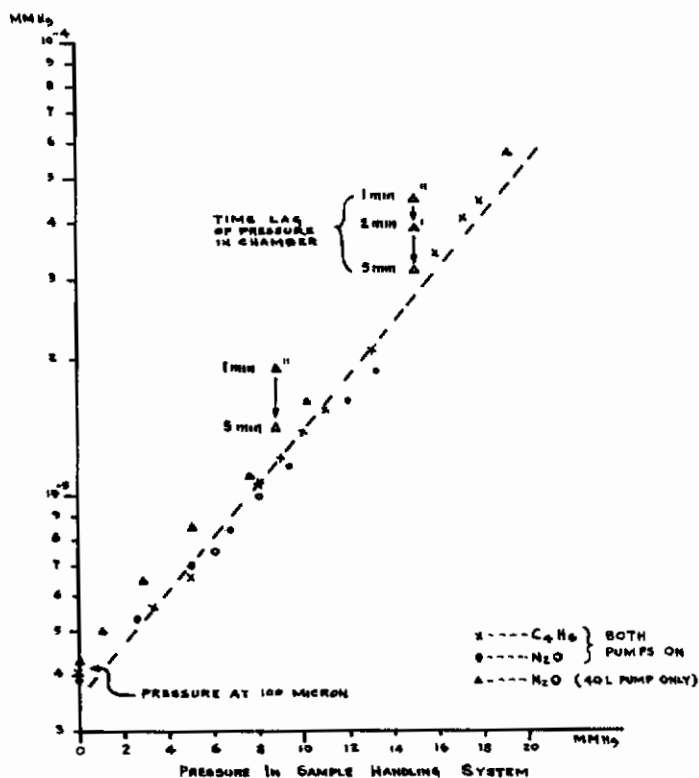


Figure 18 Calibration Chart Relation Between Pressure in Sample Flask (Dubrovin Gauge) and Pressure in Ionization Chamber (Ionization Gauge).

The alignment of the grid structure with respect to the drift tube has been accomplished by optical techniques. Two discs, each with a one mm



hole in the center were introduced into the grid structure from both ends. The image of the well collimated light beam through these holes was observed on a fine mesh at the end of the drift tube. This procedure resulted in an angular alignment between the center lines of the grid structure and the drift tube to an accuracy of better than 5 seconds.

The adjustment of the grid structure with respect to the electron gun and x-ray tube was accomplished by mechanical means. The electron gun and x-ray tube were tested separately by monitoring the beams in corresponding measuring devices. An ionization chamber with a thin aluminized Mylar window produced a current of  $3 \times 10^{-14}$  amperes. Considering the geometry of the chamber, window thickness and nature and pressure of the gas, this current corresponds to approximately  $10^8$  photons per second.

The calibration of the data handling system, essentially the time analyzer, has been accomplished in two different ways. The first method simulates the electron and ion pulses. While the base is triggered by a train of subsequent pulses, the ion pulses are represented by another train of pulses with adjustable phase shift towards the "electron" pulses. The calibration of the pulse-height analyzer for a given sawtooth length is shown in Figure 19. It can be seen from Figure 19, that the linearity of the time analyzer is very satisfactory except for the last channels. Another linearity test consisted of feeding uncorrelated ion and electron pulses into the time-to-pulse-height converter. In this case the accumulation in any particular channel is equally probable for a linear circuit. The result is then a flat top distribution.

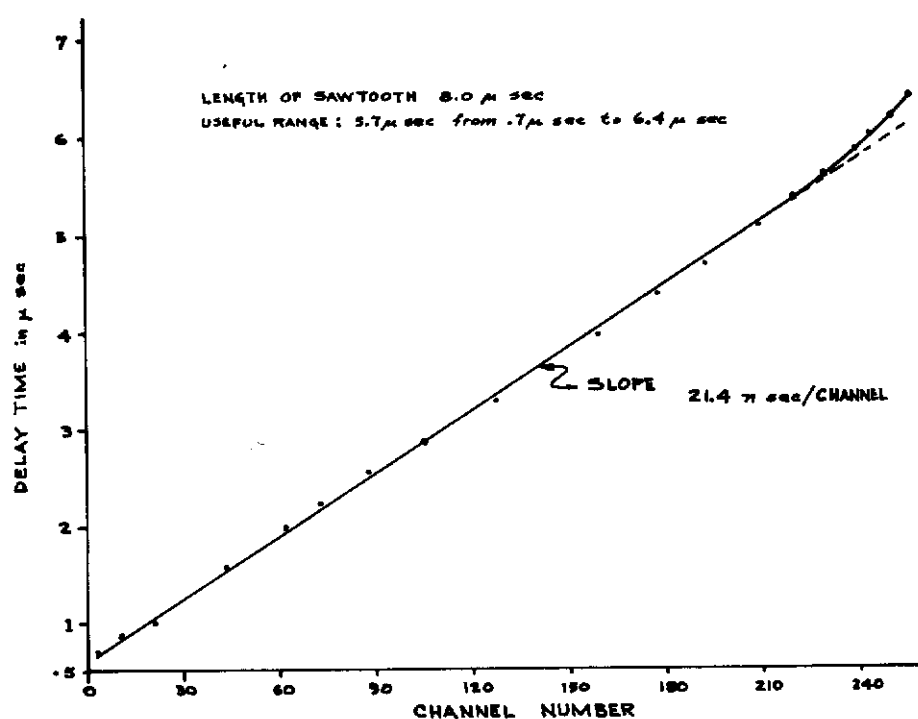


Figure 19 Calibration Chart of Pulse-height Analyzer for a Preset Sawtooth of 8 $\mu$ sec Length.

The second method is an internal calibration and consists essentially of the display of the mass spectrum of a well known simple gas such as helium, nitrogen or carbon dioxide. Knowledge of the mass number and the delay time of two or more peaks determines the entire time-to-mass scale.

## B. PERFORMANCES TESTS

The performance tests were conducted on the various units both separately and as a complete system.

The most critical information is the collection efficiency of ions and secondary electrons. The number of ionization events can be calculated when the geometry, gas pressure, intensity of the primary beam, and the ionization cross-section of the gas is known. Several tests proved that the ion collection efficiency is better than 60% and the electron efficiency is 100%.

The secondary electron collection has been carefully determined under x-ray bombardment. This was done to separate real secondary electrons of the gas phase from electrons that are scattered and ejected from metal surfaces. The dependence of the secondary electron count rate on the gas pressure has been measured. The extrapolation of the curve to zero pressure still indicated a high number of detected electrons. This part of the total count was interpreted as electrons that were not generated in the gas phase. To reduce this number, the x-ray trap and shielding were improved. This modification resulted in a considerable decrease of scattered and metal surface electrons.

In the first performance tests of the entire system residual gas and nitrous oxide were bombarded with high energy electrons. One section of the experimental spectrum is represented in Figure 20. The procedure of analysis and identification of the peaks is indicated in this figure. The notations in this recorded graph are as follows: number of counts - channel number - delay time - mass number. The print-out sheet shows the low background in those regions where no mass peak was expected. This can be seen by comparing the number of counts in channels 7 to 12. The location of the mass peaks particularly the mass numbers 28 and 40 (from residual argon) allowed the experimental establishment of the time-to-mass scale and a comparison with the calculated scale. Thus, according to equation (3) the calculated relation is  $\tau = 3.55 \sqrt{m}$  in  $\mu$  sec., while the experimentally obtained scale is  $\tau = 3.45 \sqrt{m}$  in  $\mu$  sec. for  $m$  in amu.

## C. REAGENT MATERIALS AND ENERGY DISTRIBUTION OF BOMBARDING PARTICLES

Fragmentation patterns following ionization by high energy electrons and by x-rays have been measured for nitrous oxide, butadiene, and propane. In addition nitrogen was used in calibration measurements. The minimum purities of these gases as furnished by the manufacturers are as follows:

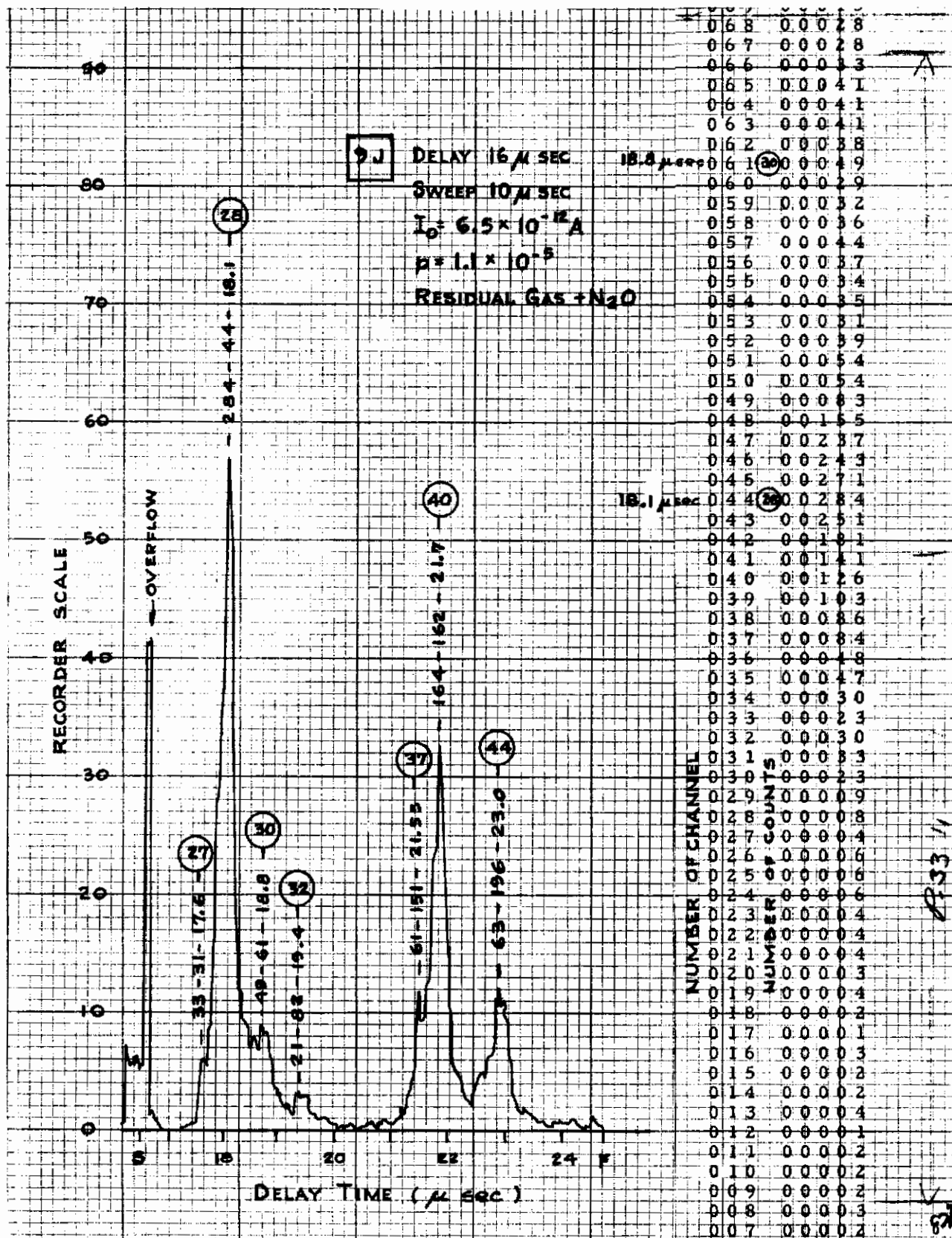


Figure 20 Experimental Data as Obtained from Data Handling System.

Nitrous oxide	98.0	per cent
Nitrogen	99.6	per cent
Propane	99.99	per cent
1, 3-Butadiene	99.4	per cent

To avoid introduction of any impurities, the sample handling system was evacuated to a pressure of 0.1 microns and then flushed with the sample gas. The sample gas was then introduced at a pressure of from 2 to 20 mm. of Hg. in the sample handling system.

The energy of the primary electron is variable over the range from 100 to 6000 electron volts with an accuracy of 0.5 per cent at any setting.

The energy spectrum of the x-ray tube depends on the high voltage, with the Bremsstrahlung x-rays ranging in energy from the window cut-off at about 1000 ev up to the energy corresponding to the high voltage on the x-ray tube. The high voltage from all the measurements to date was set at 7000 volts. In addition to the Bremsstrahlung x-radiation there is superimposed the characteristic radiation of aluminum. Thus it is expected that the x-ray spectrum is dominated by the aluminum  $K_{\alpha}$  line at about 1.5 kev with a secondary maximum due to the Bremsstrahlung at about 2.5 kev.

#### D. ION DISTRIBUTION FROM BOMBARDMENTS WITH HIGH ENERGY ELECTRONS

A knowledge of the fragmentation patterns of a molecule under high energy electron bombardment allows important correlations and comparisons with the fragmentation following ionization by x-rays. Due to the much larger cross-sections for electron ionization it is difficult to avoid a small amount of ionization in the x-ray spectrum being generated by high energy secondary electrons. Comparing the measured x-ray spectrum with the electron spectrum of similar energies assures that differences between the x-ray and electron spectra will be observed.

Butadiene, propane, and nitrous oxide have been bombarded with electrons of 1200 ev energy. The spectrum of butadiene is shown in Figure 21. The spectrum of propane is shown in Figure 22. The spectrum of butadiene contains nitrous oxide, which is used as "calibration" gas in a ratio of 4:1, the total pressure being  $1.6 \times 10^{-5}$  mm. Hg. The great abundance of the  $H_2^+$  peak is difficult to understand. Purifications of the sample gas indicated that the  $H_2$  is not contained in the sample. The background analysis also shows an  $H_2$  peak, however to a smaller extent. Also here the doubly charged peaks and peaks of low mass number are pronounced.

This enhancement of the lower mass peaks was previously observed using 600 ev primary electrons. As the primary energy increases, these effects become more pronounced. This effect is probably due to the increased amount of multiple ionization either by direct outer shell ionization of more than one electron or alternatively the inner-shell ionization of an electron followed by an Auger transition in which the excess energy is dissipated by the ejection of one or more outer shell electrons. Since multiple

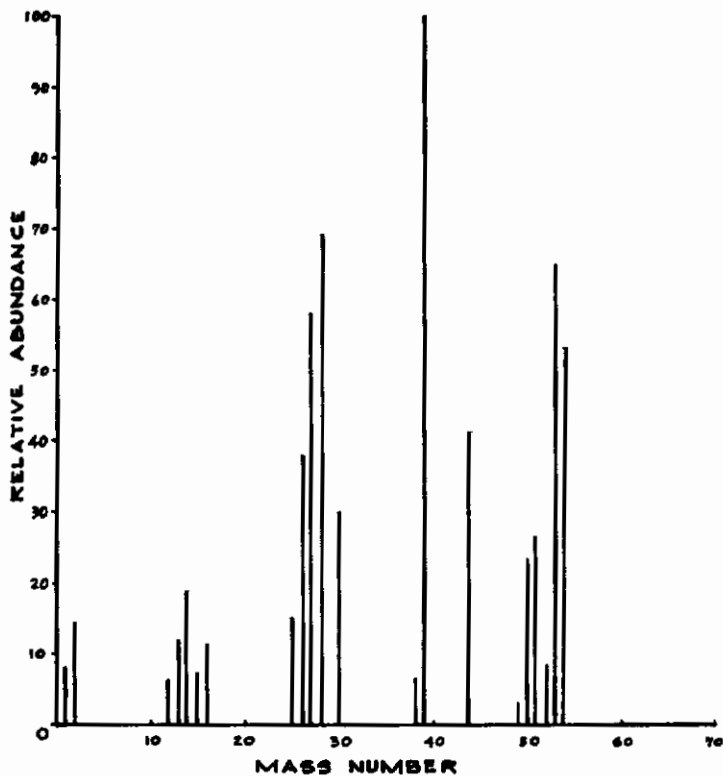


Figure 21 Spectrum of 1,3-Butadiene with Nitrous Oxide under Electron Bombardment. Electron Energy 1200 ev.

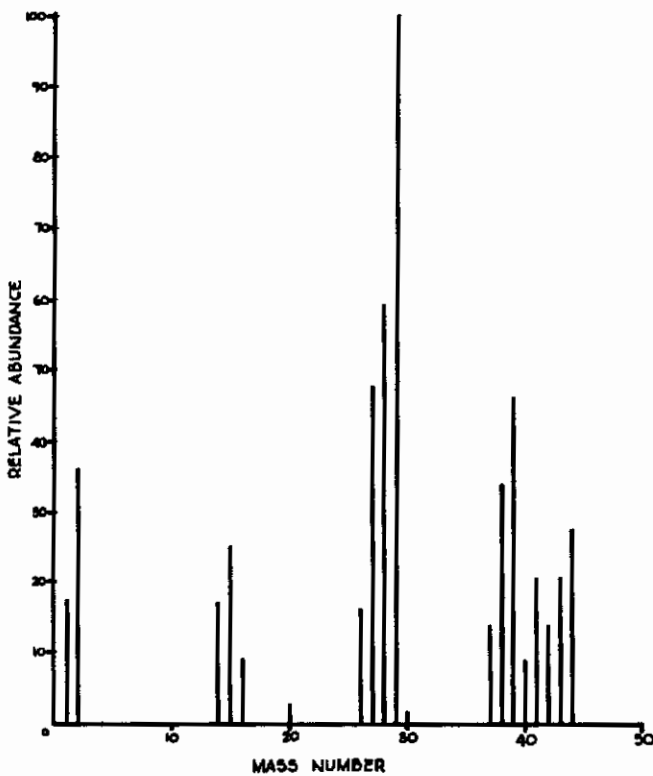
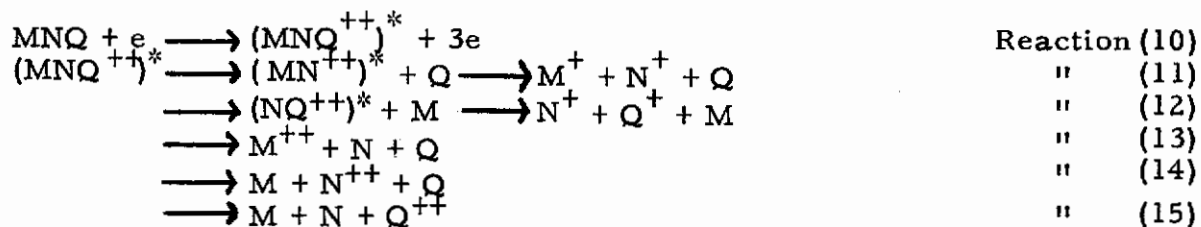


Figure 22 Spectrum of Propane Under Electron Bombardment- Electrical Energy 1200 ev.

charged large molecules tend to be unstable, the fragmentation probably proceeds rapidly along one of the paths indicated by the following reactions for a doubly charged ion.



These data show the type of reactions which may result from formation of a large multiple charged ion and show the resulting larger abundances of smaller mass and multiple charged ion which cause the observed enhancement of the low voltage electron spectrum.

#### E. INNER-SHELL IONIZATION AND ION FRAGMENTATION UNDER X-RAY BOMBARDMENT

A series of measurements were made of the ionization and fragmentation patterns of gaseous nitrous oxide and of a simple gas phase hydrocarbon, propane, under x-ray bombardment. The procedures of each run involved several steps.

The first step consisted of the adjustment of the coincidence mass spectrometer for maximum resolution using high energy electrons as bombarding particles. This procedure was required, in principle, only once for proper performance of the spectrometer. However, repetition of this procedure before each run provided, also, a reliable and fast method for determining the residual gas in the ionization chamber.

The second step was the measurement of the number of noise pulses per unit time in the electron and ion detectors in the absence of an ionizing source. This information allowed the calculation of the rate of chance coincidence from the random noise.

The third step of each run consisted of a long measurement of the spectra of the residual gas in the ionization chamber, prior to the introduction of the sample gas. These background measurements were used to correct the data for the small contributions of the residual gases. The time-converter data system made possible semi-automatic data reduction in this step. The background spectrum was stored in one half of the analyzer memory and the sample spectrum was accumulated in remaining memory of the analyzer. By partial complementing and by memory transfer, the corrected spectrum of each sample was printed directly.

During each run, the x-ray tube was operated at 7000 volts and 50 ma; these conditions introduced  $10^8$  photons per second of x-radiation into the ionization region. Also the guard plates around the x-ray trap were elevated to a sufficient potential to minimize the ejection of stray electrons.

A series of runs were made on the simple molecule, nitrous oxide, at various pressures. The final measurements are summarized in Figure 23 which shows the measured spectrum of ionic fragmentation produced by x-radiation on  $N_2O$  at a pressure of  $2.2 \times 10^{-5}$  mm. Hg.

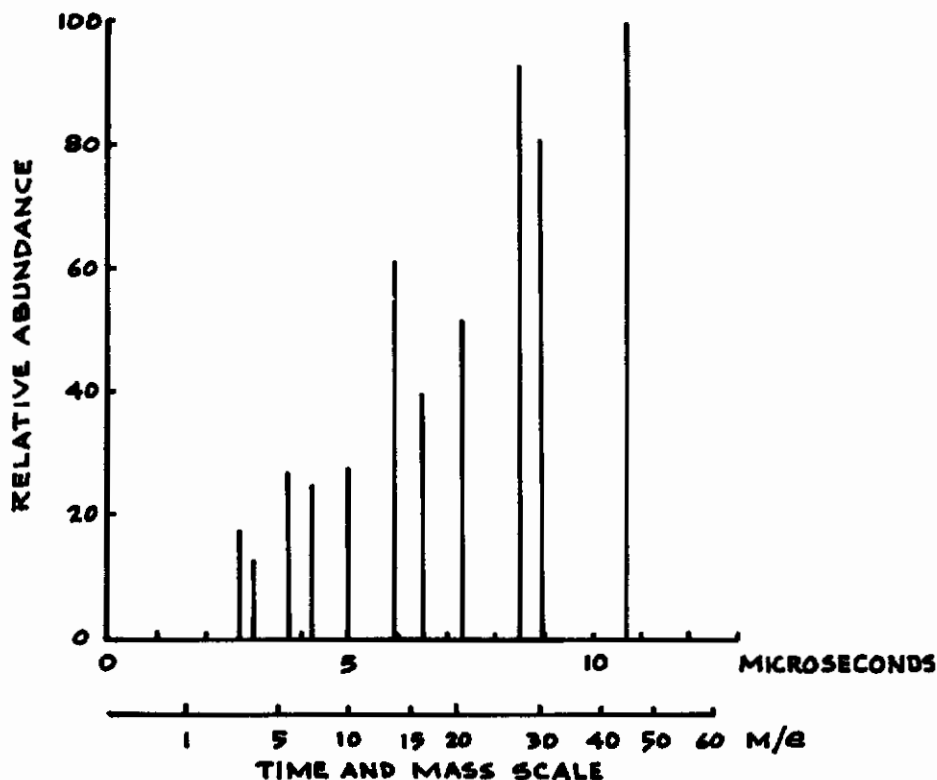
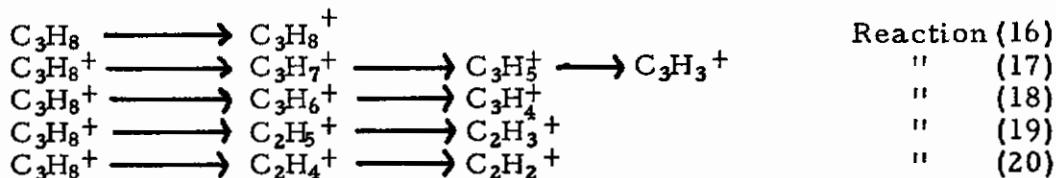


Figure 23 Spectrum of  $N_2O$  under X-ray Bombardment.

The measurements on propane are summarized in Figure 24 which shows the spectrum of ionic fragmentation produced by x-radiation on  $C_3H_8$  at  $2.8 \times 10^{-5}$  mm. Hg. At this pressure ion-molecule reactions were negligible.

Since inner shell ionization is much more probable from x-ray impact than from electron impact, the sequence of reactions leading to the observed fragmentation patterns may be quite different. Thus for electron impact on propane a sequence of reactions which accounts for about 98 per cent of the fragments observed in the mass spectrum may be written as follows:



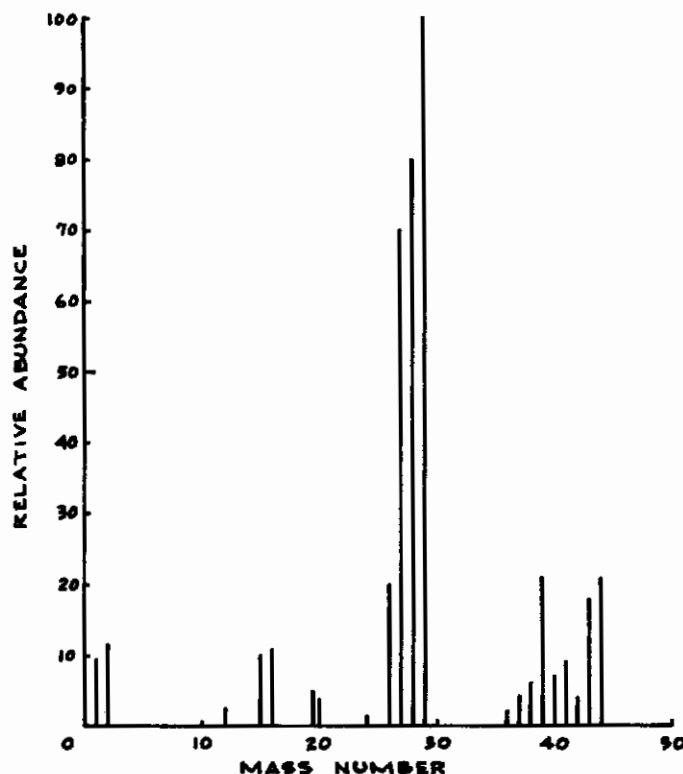


Figure 24 Spectrum of Propane Under X-ray Bombardment.

In these equations the electrons and the neutral species are not shown. The quasi-equilibrium theory of mass spectra, based on this reaction scheme, predicts rather well the experimental mass spectra produced by ordinary electron impacts.

In the case of ionization by x-radiation the fragmentation of propane may proceed along quite different reaction paths. The probable interaction between a photon of x-radiation and a molecule of propane is the photoelectric ejection of an inner shell electron. This reaction may be represented as



Since the ejected electron came from an inner shell, the resulting ion is left in an extremely excited state. This excitation energy will probably be dissipated by an Auger transition in which the vacancy in the inner shell is filled by an outer shell electron and the excess energy ejects one or more electrons from the outer shells.

On the basis of this theory we expect that the fragmentation reactions of propane following x-ray impact start from an excited multiple charged ion rather than a singly charged ion. Thus, the reaction scheme for single ionization is no longer valid and must be replaced by a scheme of reactions which takes into account the multiplicity of charge of the primary ion. From the



great many additional possible reactions which may be contributing to the observed fragmentation patterns, we consider only those involving doubly charged propane. The corresponding mass numbers are also given in the following table.

Table 1  
Mass Numbers from Primary and Secondary Reactions

Primary Reactions	Observed Masses
$C_3H_8^{++} \longrightarrow C_3H_7^{++} + H$	21.5
$\longrightarrow C_3H_7^+ + H^+$	43 and 1
$\longrightarrow C_3H_6^{++} + H_2$	21
$\longrightarrow C_3H_6^+ + H_2^+$	42 and 2
$\longrightarrow C_2H_5^{++} + CH_3$	14.5
$\longrightarrow C_2H_5^+ + CH_3^+$	29 and 15
$\longrightarrow C_2H_5 + CH_3^{++}$	7.5
$\longrightarrow C_2H_4^{++} + CH_4$	14
$\longrightarrow C_2H_4^+ + CH_4^+$	28 and 16
$\longrightarrow C_2H_4 + CH_4^{++}$	8
<u>Secondary Reactions</u>	
$C_3H_7^{++} \longrightarrow C_3H_5^{++} + H_2$	20.5
$\longrightarrow C_3H_5^+ + H_2^+$	41 and 2
$C_3H_6^{++} \longrightarrow C_3H_4^{++} + H_2$	20
$\longrightarrow C_3H_4^+ + H_2^+$	40 and 2
$C_2H_5^{++} \longrightarrow C_2H_3^{++} + H_2$	13.5
$\longrightarrow C_2H_3^+ + H_2^+$	27 and 2
$C_2H_4^{++} \longrightarrow C_2H_2^{++} + H_2$	13
$\longrightarrow C_2H_2^+ + H_2^+$	26 and 2

The interpretation of the observed spectra is complicated by this large number of reactions which must be considered. The relatively high experimental abundances of the  $H^+$  and  $H_2^+$  fragments together with the relatively small difference in the abundance of the large parts of the x-ray spectrum relative to the electron spectrum seem to indicate that the reactions in which the charge is divided between the two fragments are favored over those in which both charges remain with a single fragment. The relatively high abundance of  $CH_3^+$  and  $CH_4^+$  appear to be consistent with this hypothesis. Although it is impossible at this time to assess accurately the effects of all the possible reactions on the observed fragmentation patterns, the following reactions appear to be the most reasonable dominant primary reactions,



These reactions together with the secondary and tertiary reactions shown in the single charge scheme are sufficient to account for almost all of the abun-

dant peaks observed in the experimental x-ray ionization spectrum summarized in Figure 24.

Further theoretical interpretation is planned in the future program as soon as enough additional data are obtained. The present program has accomplished the x-ray fragmentation measurements on propane and on nitrous oxide and has shown feasibility. The spectra are consistent with a reasonable theoretical description. The next program will concentrate on (1) obtaining much more data on a number of molecules, particularly an iso-electronics series, and (2) on doing the detailed theoretical treatment which will then be warranted.

## Section II. SECONDARY ELECTRON SPECTRA FROM BOMBARDMENT OF GASES WITH ELECTRONS

### I. INTRODUCTION

The energy distribution of the secondary electrons emitted when molecules are ionized by electron impact are of fundamental importance to radiation effects on materials in at least two ways. The first of these is connected with theoretical calculations of the products of radiation-induced reactions. These calculations are based on the assumptions that ion-molecule reactions are the primary reaction mechanism, and that the steady state distribution of ions can be inferred from mass spectra of the material irradiated. Some successful calculations of this kind have been reported in which the 50 or 70 volt mass spectrum was arbitrarily chosen as representative of the ion distribution. The question of the validity of such calculation hinges on a knowledge of the steady state energy distribution of the ionizing particles. Since it is now well established that in an irradiation by high energy particles most of the ionization is produced by the secondary electrons and electrons of succeeding generations, the composite steady state electron energy distribution is sufficient. However, any attempt to calculate this composite distribution depends upon a detailed knowledge of the secondary electron energy distribution over a wide range of primary electron energies. For this reason, secondary electron energy distribution is a necessary step to a basic understanding of the complex problems of radiation chemistry and physics.

The other important application of the secondary electron energy distribution is that of the kinetics of unimolecular dissociations of polyatomic molecule-ions in the mass spectrometer. In this connection, we must know the excitation energy distribution of dissociating molecule-ions. A knowledge of the energy and angular distributions of the secondary electrons, together with the known energy of the primary electron producing the ionization, allows an accurate determination of the excitation distributions.

In the present studies emphasis was placed on measuring the secondary electron energy distribution of those secondary electrons ejected nearly perpendicularly to the primary beams using primary ionizing electrons in the energy range of 320 to 1000 ev. This measurement was done in the coincidence mass spectrometer by detecting the electrons which are sufficiently energetic to surmount a potential "hill", whose height may be varied to obtain the spectrum. In this way the integral electron energy spectrum may be measured. The electrons are not counted directly. By using the coincidence principle, the number of ions are counted that are in the correct delayed coincidence with the detected electrons. This technique removes the common error of incorrectly including in the spectrum electrons which originate from sources other than the ionization process under consideration.

### II. THEORY OF THE IONIZING COLLISIONS OF ELECTRONS ON MOLECULES

At present an extensive theoretical treatment of the ionizing collisions of electrons with complex molecules is not feasible. Although the first Born

approximation provides an adequate tool, provided the energy of the impacting electrons is sufficiently large, the wave functions required for its application are known with sufficient accuracy only for some simple cases, i. e. atomic hydrogen and helium. Therefore, the fundamental experimental approach of the current program is necessary to provide the quantitative information needed for understanding the effects of ionizing collisions on molecules.

However, approximate calculations for more complex atoms and molecules indicate that the distributions of energy and angle of the scattered primary electrons and the ejected secondary electrons are qualitatively similar. Those similarities may be summarized as follows:

- (1) For small velocities of the ejected electrons, the angular distribution of the scattered electrons fall rapidly with an increasing angle of scattering.
- (2) For high velocities of the ejected electron, the angular distributions of both the ejected electron and the scattered electron show relatively sharp maxima corresponding to conservation of momentum between electrons.
- (3) The probability of energy transfer from the incident electron to the ion and secondary electron rises rapidly to a maximum at a relatively low energy of ejection, and falls off quite rapidly with increasing energy.

Since it is expected that the distributions for more complex atoms and molecules should be qualitatively similar for those for atomic hydrogen, some calculated distributions of this particularly simple case provide a basis for comparison and interpretation of the experimental data obtained from the more complex situations.

An ionizing collision may be represented by a vector diagram as shown in Figure 25. The incident electron with momentum  $P_0$  collides with a molecule and ionizes it by causing a bound electron to be ejected with momentum  $P_1$ . The scattered primary leaves with momentum  $P_2$ .  $P_3$  is the change in momentum of the incident electron and  $P_4$  is the momentum transferred to the ion. It can easily be shown that the kinetic energy transferred to the ion is always very small although the momentum transferred may be quite appreciable. In the extreme case of a "head-on" collision, the maximum momentum and energy are transferred to the ion. In this case,

$$P_4 \leq 2P_0 \quad (10)$$

# Contrails

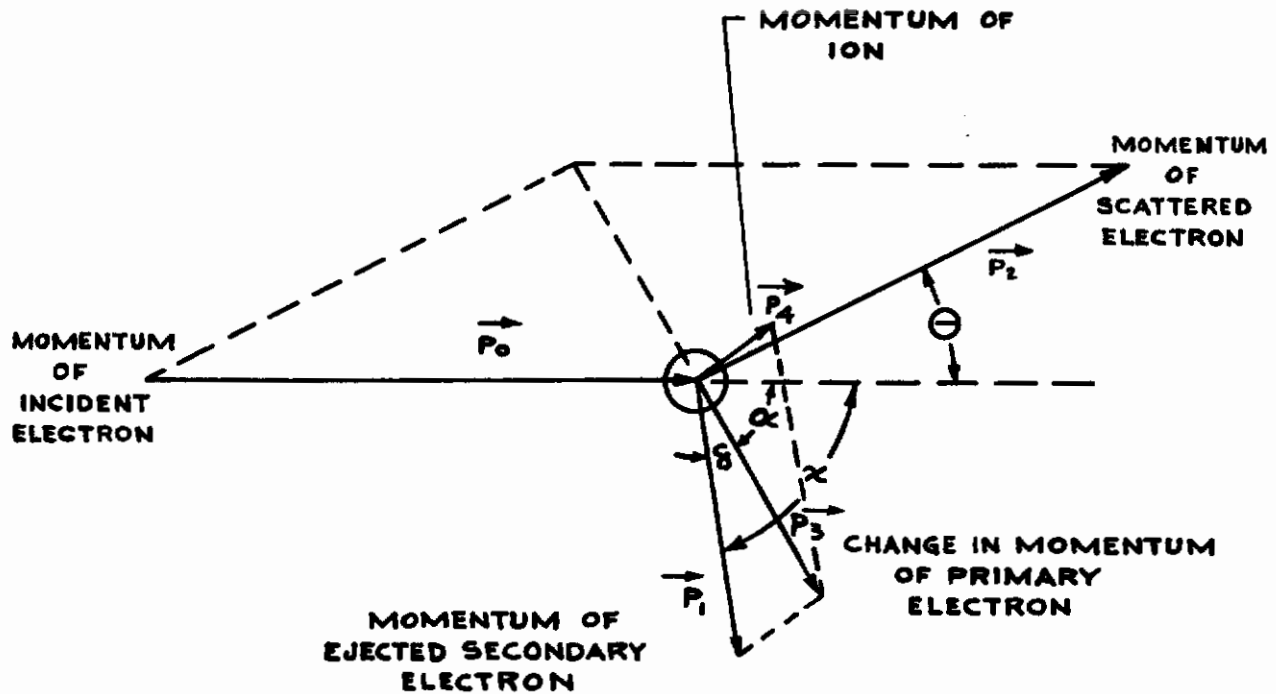


Figure 25 Vector Diagram of an Ionizing Collision.

and the kinetic energy of the ion is

$$T_4 = \frac{P_4^2}{2M_4} \leq \frac{4P_0^2}{2M_4} = \frac{4M_0}{M_4} T_0 \quad (11)$$

where  $T_0$  is the kinetic energy of the incident electron and  $M_0$  and  $M_4$  are the masses of the electron and ion respectively. Thus, even for the extreme case of atomic hydrogen the maximum possible transfer of kinetic energy is only 0.2 per cent of the energy of the incident electron.

Further consideration of the geometry of the collision shown in Figure (26) also yields the relation

$$P_3^2 = P_0^2 + P_2^2 - 2P_0P_2 \cos \theta \quad (12)$$

where  $\theta$  is the angle between the initial and final directions of the scattered electron. The direction of the change in momentum of the scattered electron is given by the angle  $\alpha$  where

$$\cos \alpha = \frac{P_1 - P_2 \cos \theta}{P_3} \quad (13)$$

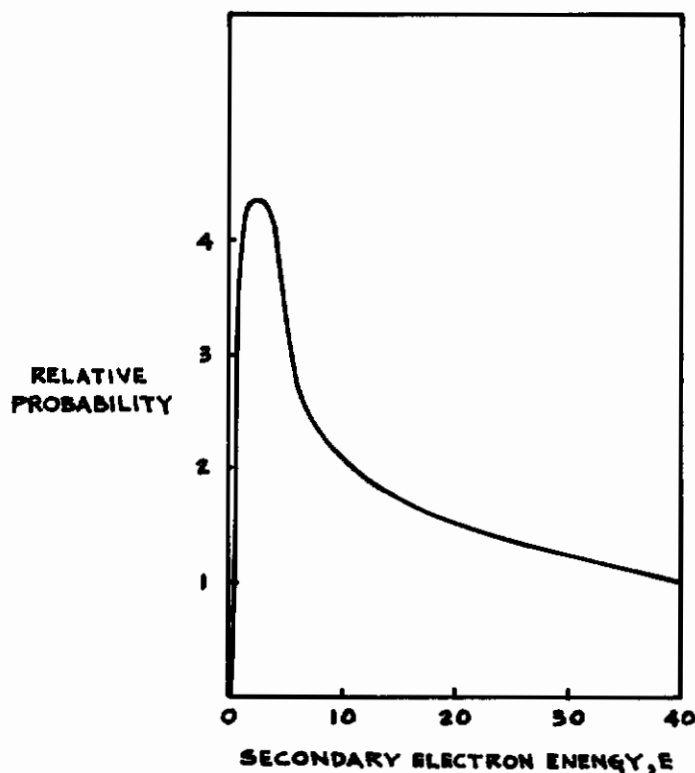


Figure 26 Calculated Differential Energy Spectrum of Secondary Electrons Ejected Perpendicular to the Primary Beam for Atomic Hydrogen at a Primary Electron Energy of 1000 ev.

Further analysis of an ionizing collision requires the application of quantum-mechanical collision theory, (8). The first Born approximation is valid provided the energy of the incident electron is sufficiently large compared to the ionization potential. Under this approximation the differential cross-section for the ionizing collision illustrated in Figure 30 is given by

$$I = \frac{2^3 a_0^3}{\pi} \cdot \frac{k_1 k_2}{k_0 k_3} \cdot \frac{\exp \left[ -\left( \frac{2}{k_1} \right) \arctan \left( \frac{2k_1}{1+k_3^2/k_1^2} \right) \right]}{\left( 1 - \rho^{-2\pi/k_1} \right) \left( 1 + k_3^2 + k_1^2 - 2k_3 k_1 \cos \delta \right)^4} \quad (14)$$

$$\times \frac{\left[ \left( k_3 - k_1 \cos \delta \right)^2 + 1 \right]}{\left( 1 + k_3^2 - k_1^2 \right)^2 + 4k_1^2}$$

where  $k_i = \frac{P_i a_0}{h}$

is the dimensionless wave number in units of reciprocal Bohr radii for an electron with momentum  $P_i$ , and  $\delta$  is the angle between the direction of the ejected electron and the change in momentum of the scattered electron. It can easily be shown from equation (14) that a relative maximum in the cross-section  $I$  occurs for  $\delta = 0$ , corresponding to conservation of momentum between electrons.

Some calculations of the differential cross-sections for ionization of hydrogen by 1000 ev electrons have been completed. The calculated differential secondary electron spectrum for electrons ejected perpendicularly to the primary beam is shown in Figure 26. This result provides a basis for semi-quantitative comparisons with the experimental data obtained for more complex molecules.

### III. EXPERIMENTAL PROCEDURE

A number of difficulties have to be overcome to measure reliably the energy spectra of the secondary electron emitted due to an ionizing collision occurring in the gas phase. These difficulties include the following: (1) Electrons from the primary beam may be scattered into the collector. (2) Secondary electrons may be collected from metal surfaces. (3) Secondary electrons may be collected from molecules other than the one being studied.

When applied to measurements in the gas phase, attempts to overcome these difficulties have been unsuccessful when conventional methods, similar to those used in measuring secondary electron spectra from solids, were used.

The use of the Coincidence Mass Spectrometer surmounts those difficulties by accepting only those electrons which are properly correlated with the ion formed.

A schematic representation of the Coincidence Mass Spectrometer as modified for the measurement of secondary electron spectra is shown in Figure 27. To measure the secondary electron spectra for a given molecule, a high purity sample of the gas is injected into the ionization chamber through the narrow capillary connecting the sample handling system to the ionization chamber. The pressure of the gas in the sample handling system is adjusted so that the pressure of the sample gas in the ionization chamber is maintained at one to two orders of magnitude above the residual gas pressure. Since the residual gas pressure is normally about  $5 \times 10^{-7}$  mm. of Hg. or less, the normal range of operating pressures is from  $5 \times 10^{-6}$  to  $5 \times 10^{-5}$  mm. of Hg. To further improve the purity of the gas studied, the ionization chamber may be flushed several times with the sample gas to further reduce the partial pressure of the residual gas.

During a measurement, the electron gun emits a narrow, collimated beam of electrons which are accelerated down the center of the region of the ionization chamber bounded by the grids G2 and G3. Grid G2 is maintained at a positive potential relative to the electron beam while G3 is negative. Thus, when an ionization occurs in the region in front of the fine mesh windows in G2 and G3, the secondary electron is accelerated toward the electron detector while the ion is accelerated down the drift tube toward the ion detector. The region between G3 and G4 provides an additional ion accelerating field which may be used to reduce the variation in travel time of ions of the same mass. The variation may result from the finite width of the primary electron beam, or from the initial kinetic energy of the ions.

In this manner, the time interval between the detection of the secondary electron and the corresponding ion provides a measure of the mass of the ion.

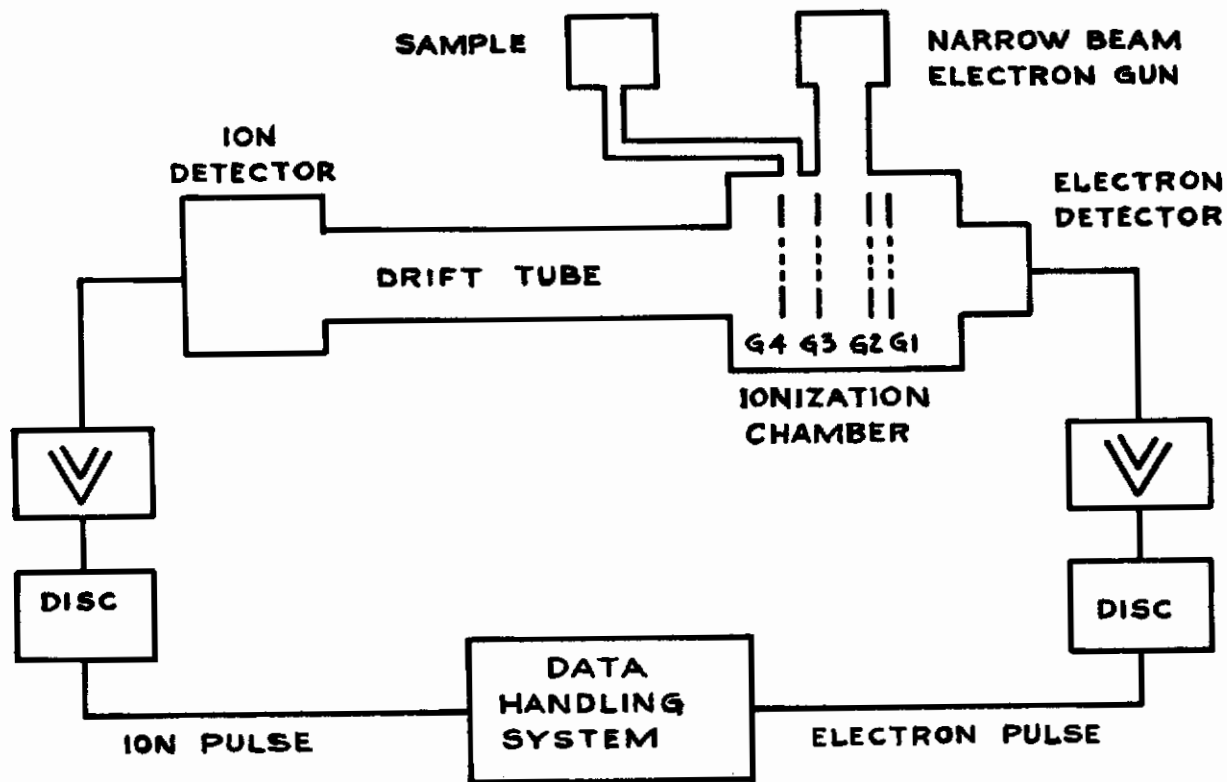


Figure 27 Schematic Representation of the Coincidence Mass Spectrometer as Modified for Secondary Electron Energy Measurements.

When an ion or electron collides with the first dynode of the detector, a pulse is produced which is fed through a discriminator to the data handling system.

When the Coincidence Mass Spectrometer is used to measure secondary electron spectra, an additional grid G1 is placed between the ionization region and the electron detector. Energy analysis of the ejected secondary electrons is performed by varying the potential of grid G1. When the potential of grid G1 is negative with respect to the primary beam by a voltage  $V$ , only those electrons which are ejected by the ionization process with energy exceeding  $V$  electron volts can pass G1 and reach the electron detector. Only those ions resulting from an ionization in which the energy of the ejected electron exceeded  $V$  are detected in the proper time correlation with a detected secondary electron. Thus, the number of ions of a particular mass (or delay time) is measured as a function of the negative potential  $V$  on grid G1. The use of this method not only allows positive determination of the molecule ionized, but also prevents the improper inclusion of electrons scattered from the primary beam or ejected from metal surface, since in these cases no ion is detected.

#### IV. RESULTS

A series of measurements of secondary electron energy spectra from



320 to 1000 electron volts have been completed. A list of the materials studied together with their minimum purities as provided by the manufacturer is given in Table 2. To further insure purity of the samples measured, the sample handling system and the ionization chamber were flushed several times with the sample gas immediately prior to final injection of the sample to be measured. Also the pressure of sample gas for all of the measurements reported was maintained in the ionization chamber at 20 to 100 times the residual gas pressure in the system which during the time of these measurements was consistently less than  $10^{-6}$  mm. Hg.

Table 2  
Materials Used in Secondary Electron Spectra  
Measurements

<u>Material</u>	<u>Minimum Purity (%)</u>
Nitrogen	99.9
Argon	99.9
n-Butane	99.99
1,3-Butadiene	99.4
n-Pentane	99.0
Cyclohexane	99.0
Propane	99.99

The results of these measurements are summarized in Tables 3 through 13. The first two columns present the raw data corrected only for fluctuations in total ionization. The retarding potential is the measured negative potential of the grid G1 (see Figure 27) relative to ground. The second column gives the measured number of electrons, corresponding to a particular ion, which were sufficiently energetic to surmount the potential barrier imposed by the retarding potential on G1. The potentials on grids G2 and G3 were adjusted so that the potential of the point where the ionization occurred was at ground. Thus, the minimum electron energy, as given in the third column of the tables corresponds to the measured retarding potential. The relative number of electrons with energy greater than the given energy, tabulated in the fourth column of the tables, is obtained from the raw data by multiplying the raw counts by a suitable constant multiplier so that the number with energy greater than zero is normalized to 100 per cent.

The measured secondary electron spectra for several molecules are plotted in Figures 28 through 41. The data plotted in Figures 32 through 41 correspond to the normalized data of Tables 3 through 13 respectively.

The data shown in Figures 28 through 31 are for some preliminary measurements which were made without employing the coincidence principle. These data show a considerable enhancement of the low energy portion of the spectrum relative to the coincidence data. For example, for propane with 800 ev primary electron energy, a comparison of Figure 31, a non-coincidence measurement, with Figure 35, the same measurement using the coincidence principle, shows this quite clearly. For the non-coincidence measurement less than 10 per cent of the secondary electrons show energies in excess of 10 ev, while for the coincidence measurement more than 30 per cent of the secondary electrons have energies larger than 10 ev.

Table 3

Secondary Electron Energy Spectrum for N<sub>2</sub> Using  
320 ev Primary Electron Energy

Raw Data		Normalized Data	
<u>Retarding Potential (1)</u>	<u>Counts/Min. (2)</u>	<u>Secondary Electron Energy (3)</u>	<u>Per Cent with Greater Energy(4)</u>
0	1001	0	100
1	967	1	97
2	953	2	95
3	995	3	99
4	915	4	92
5	903	5	90
6	875	6	87
10	623	10	62
15	404	15	40
20	254	20	25
25	136	25	14
30	115	30	12
40	109	40	11
50	87	50	9
60	62	60	6
70	63	70	6

(1) Measured Relative to Potential at Primary Electron Beam.

(2) One Minute Counts.

(3) Units of Electron Volts.

(4) In Per Cent of Raw Counts for Zero Retarding Potential

Table 4

Secondary Electron Spectrum for N<sub>2</sub> Using  
800 ev Primary Electron Energy

Raw Data		Normalized Data	
<u>Retarding Potential (1)</u>	<u>Counts/Min. (2)</u>	<u>Secondary Electron Energy(3)</u>	<u>Per Cent with Greater Energy(4)</u>
0	658	0	100
1	640	1	97
2	671	2	102
3	544	3	82
4	540	4	82
5	557	5	85
6	489	6	74
8	476	8	73
10	401	10	61
12	338	12	52
15	312	15	47
20	226	20	35
25	169	25	26
30	163	30	24
40	127	40	20
50	135	50	20
60	149	60	23

(1) Measured Relative to Potential at Primary Electron Beam.

(2) One Minute Counts.

(3) Units of Electron Volts.

(4) In Per Cent of Raw Counts for Zero Retarding Potential.

Table 5

Secondary Electron Energy Spectrum for Propane  
Using 320 ev Primary Electron Energy

Raw Data		Normalized Data	
<u>Retarding Potential (1)</u>	<u>Counts/Min. (2)</u>	<u>Secondary Electron Energy(3)</u>	<u>Per Cent with Greater Energy(4)</u>
0	261	0	100
1	268	1	103
2	245	2	94
3	233	3	89
4	241	4	92
5	230	5	88
6	235	6	90
8	204	8	78
10	194	10	74
12	166	12	64
15	130	15	50
20	104	20	40
30	35	30	13
40	26	40	10
50	21	50	8
60	15	60	6
70	14	70	5

- (1) Measured Relative to Potential at Primary Electron Beam.  
(2) One Minute Counts.  
(3) Units of Electron Volts.  
(4) In Per Cent of Raw Counts for Zero Retarding Potential.

Table 6

Secondary Electron Energy Spectrum for Propane  
Using 800 ev Primary Electron Energy

Raw Data		Normalized Data	
<u>Retarding Potential (1)</u>	<u>Counts/Min. (2)</u>	<u>Secondary Electron Energy (3)</u>	<u>Relative Number (4)</u>
0	287	0	100
1	276	1	96
2	252	2	88
3	209	3	73
4	159	4	55
5	157	5	55
6	121	6	42
8	122	8	42
10	126	10	44
12	98	12	34
15	59	15	21
20	54	20	19
30	40	30	14
40	47	40	16
50	37	50	13
60	37	60	13
70	39	70	14

(1) Measured in Volts Negative Relative to Electron Beam.

(2) One Minute Counts.

(3) Units of Electron Volts.

(4) In Per Cent of Raw Counts for Zero Retarding Potential.

Table 7

Secondary Electron Energy Spectrum for N<sub>2</sub> Using  
1000 ev Primary Electron Energy

Raw Data		Normalized Data	
<u>Retarding Potential (1)</u>	<u>Counts/Min. (2)</u>	<u>Secondary Electron Energy (3)</u>	<u>Per Cent with Greater Energy (4)</u>
0	1065	0	100
2	1000	2	93
4	935	4	89
6	940	6	90
10	837	10	79
15	712	15	69
20	532	20	50
30	362	30	35
40	305	40	29

- (1) Measured in Volts Negative Relative to Electron Beam.
- (2) One Minute Counts.
- (3) Units of Electron Volts.
- (4) In Per Cent of Raw Counts for Zero Retarding Potential.

Table 8

Secondary Electron Energy Spectrum for Argon Using  
1000 ev Primary Electron Energy

Raw Data		Normalized Data	
<u>Retarding Potential (1)</u>	<u>Counts/Min. (2)</u>	<u>Secondary Electron Energy (3)</u>	<u>Per Cent with Greater Energy (4)</u>
0	765	0	100
2	786	2	103
4	774	4	101
6	714	6	93
8	753	8	98
10	662	10	87
12	657	12	86
15	598	15	78
20	483	20	63
30	361	30	47
40	271	40	35

- (1) Measured in Volts Negative Relative to Electron Beam.
- (2) One Minute Counts.
- (3) Units of Electron Volts.
- (4) In Per Cent of Raw Counts for Zero Retarding Potential.

Table 9

Secondary Electron Energy Spectrum for Propane  
Using 1000 ev Primary Electron Energy

Raw Data		Normalized Data	
<u>Retarding Potential (1)</u>	<u>Counts/Min. (2)</u>	<u>Secondary Electron Energy (3)</u>	<u>Per Cent with Greater Energy (4)</u>
0	527	0	100
2	473	2	90
4	484	4	92
6	465	6	88
8	498	8	94
10	419	10	79
12	331	12	63
15	334	15	63
20	187	20	35
30	116	30	22
40	103	40	19

- (1) Measured in Volts Negative to Electron Beam.
- (2) One Minute Counts.
- (3) Units of Electron Volts.
- (4) In Per Cent of Raw Counts for Zero Retarding Potential.

Table 10

Secondary Electron Energy Spectrum for n-Butane  
Using 1000 ev Primary Electron Energy

Raw Data :		Normalized Data	
<u>Retarding Potential(1)</u>	<u>Counts/Min.(2)</u>	<u>Secondary Electron Energy (3)</u>	<u>Per Cent with Greater Energy (4)</u>
0	630	0	100
2	611	2	97
4	700	7	111
6	592	6	94
10	508	10	81
15	283	15	45
20	280	20	45
30	131	30	21
40	62	40	10

- (1) Measured in Volts Negative to Electron Beam.
- (2) One Minute Counts.
- (3) Units of Electron Volts.
- (4) In Per Cent of Raw Counts for Zero Retarding Potential.

Table 11

Secondary Electron Energy Spectrum for n-Pentane  
Using 1000 ev Primary Electron Energy

Raw Data		Normalized Data	
<u>Retarding Potential (1)</u>	<u>Counts/Min. (2)</u>	<u>Secondary Electron Energy (3)</u>	<u>Per Cent with Greater Energy (4)</u>
0	349	0	100
2	330	2	95
4	273	4	78
6	184	6	53
8	183	8	52
10	141	10	40
12	98	12	28
15	72	15	21
20	36	20	10
30	28	30	8
40	20	40	6

- (1) Measured in Volts Negative to Electron Beam.
- (2) One Minute Counts.
- (3) Units of Electron Volts.
- (4) In Per Cent of Raw Counts for Zero Retarding Potential.

Table 12

Secondary Electron Energy Spectrum for 1, 3-Butadiene  
Using 1000 ev Primary Electron Energy

Raw Data		Normalized Data	
<u>Retarding Potential (1)</u>	<u>Counts/Min. (2)</u>	<u>Secondary Electron Energy (3)</u>	<u>Per Cent with Greater Energy (4)</u>
0	620	0	100
2	580	2	93
4	600	4	97
6	330	6	53
10	280	10	45
15	270	15	43
20	130	20	21
30	110	30	18
40	80	40	13

- (1) Measured in Volts Negative to Electron Beam.
- (2) One Minute Counts.
- (3) Units of Electron Volts.
- (4) In Per Cent of Raw Counts for Zero Retarding Potential.



Table 13

Secondary Electron Energy Spectrum for Cyclohexane  
Using 1000 ev Primary Electron Energy

Raw Data		Normalized Data	
<u>Retarding Potential (1)</u>	<u>Counts/Min. (2)</u>	<u>Secondary Electron Energy (3)</u>	<u>Per Cent with Greater Energy (4)</u>
0	547	0	100
2	564	2	103
4	519	4	95
6	459	6	84
8	420	8	77
10	386	10	71
12	420	12	77
15	354	15	65
20	328	20	60
30	221	30	40
40	149	40	27

- (1) Measured in Volts Negative to Electron Beam.
- (2) One Minute Counts.
- (3) Units of Electron Volts.
- (4) In Per Cent of Raw Counts for Zero Retarding Potential.

This enhancement of the low energy portion of the spectrum in the non-coincidence measurements is very probably due to the predominately low-energy electrons which are emitted from a metal surface when bombarded with electrons. These results illustrate again the necessity for using the coincidence principle to obtain reliable measurements from materials in the gas phase.

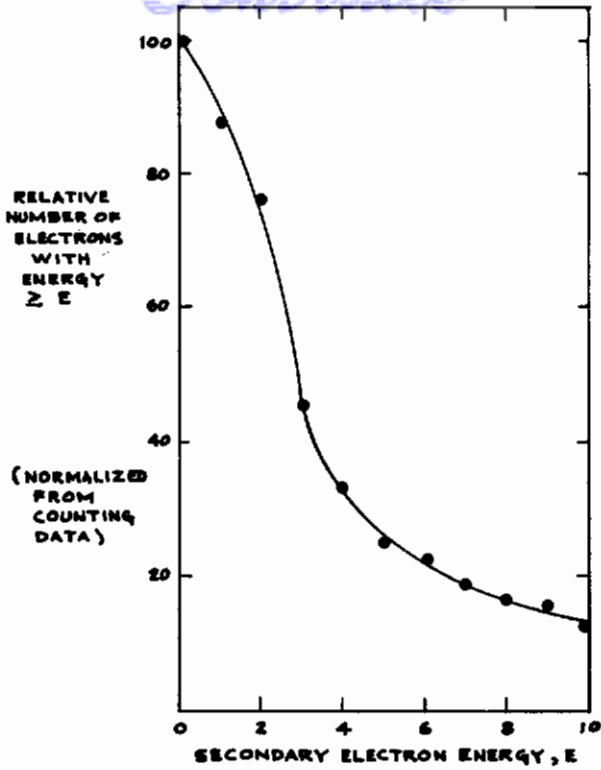


Figure 28 Integral Secondary Electron Spectra for  $N_2$  Using 500 Electron Volt Primary Electrons.

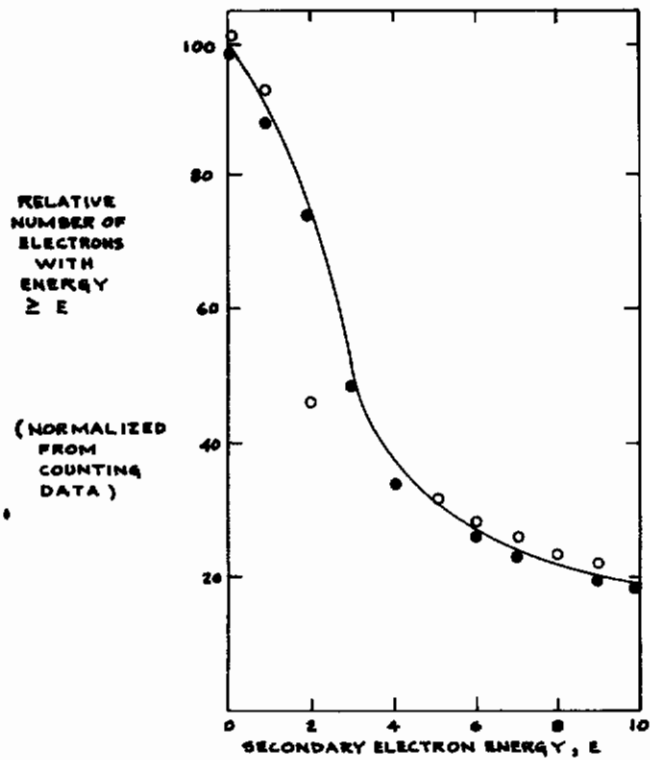


Figure 29 Integral Secondary Electron Spectra for  $N_2$  Using 600 Electron Volt Primary Electrons. Results of Two Separate Runs.

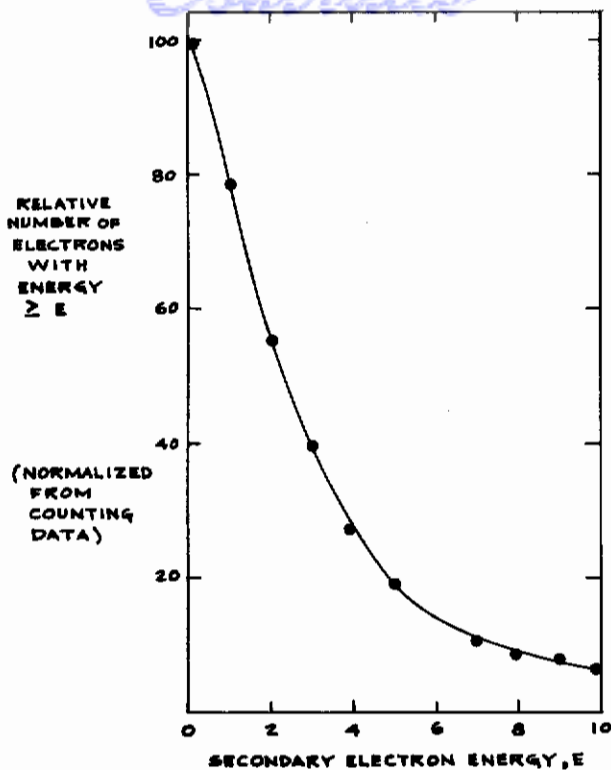


Figure 30 Integral Secondary Electron Spectra of Propane Using 400 Electron Volt Primary Electrons.

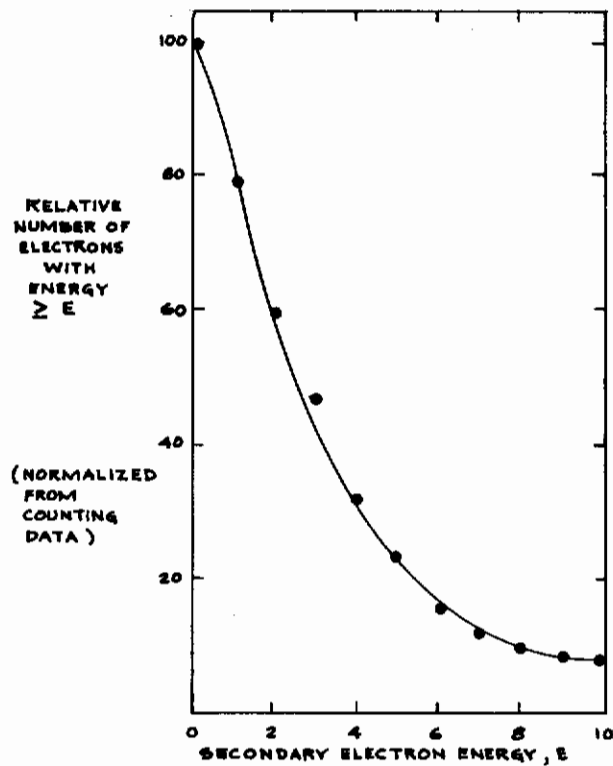


Figure 31 Integral Secondary Electron Spectra of Propane Using 800 Electron Volt Primary Electrons.

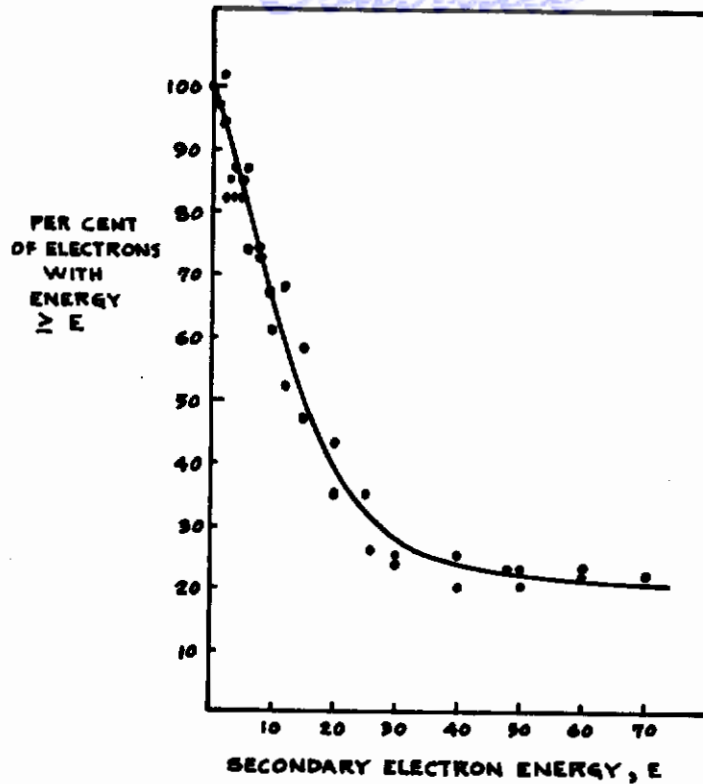


Figure 32 Secondary Electron Spectrum of  $N_2$  Using 800 eV Primary Electron Energy

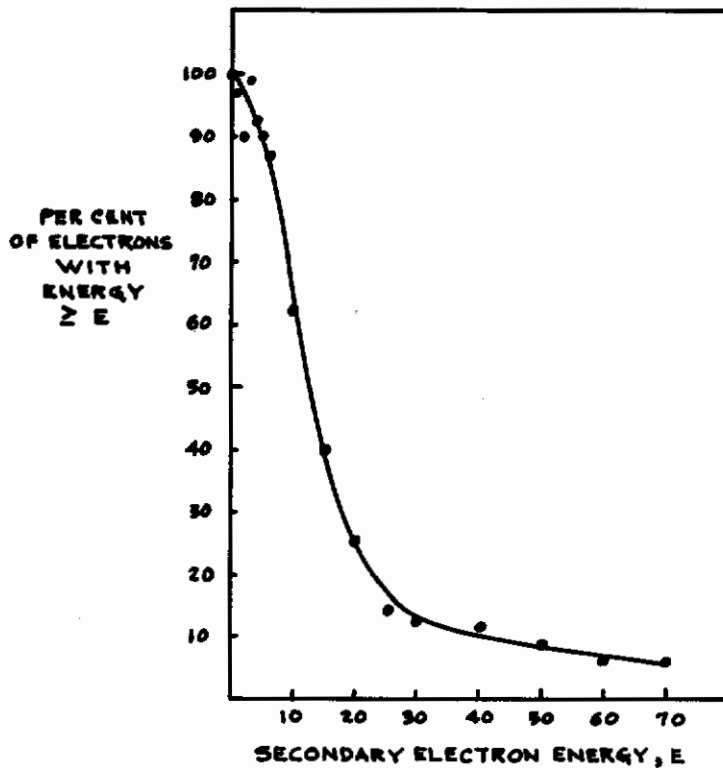


Figure 33 Secondary Electron Spectrum of  $N_2$  Using 320 eV Primary Electron Energy.

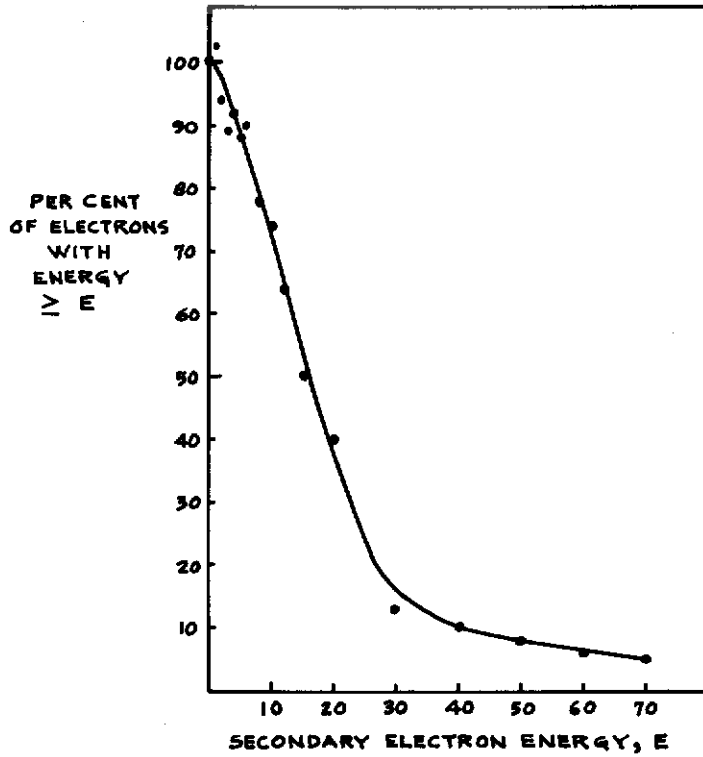


Figure 34 Secondary Electron Spectrum of Propane Using 320 eV Primary Electron Energy.

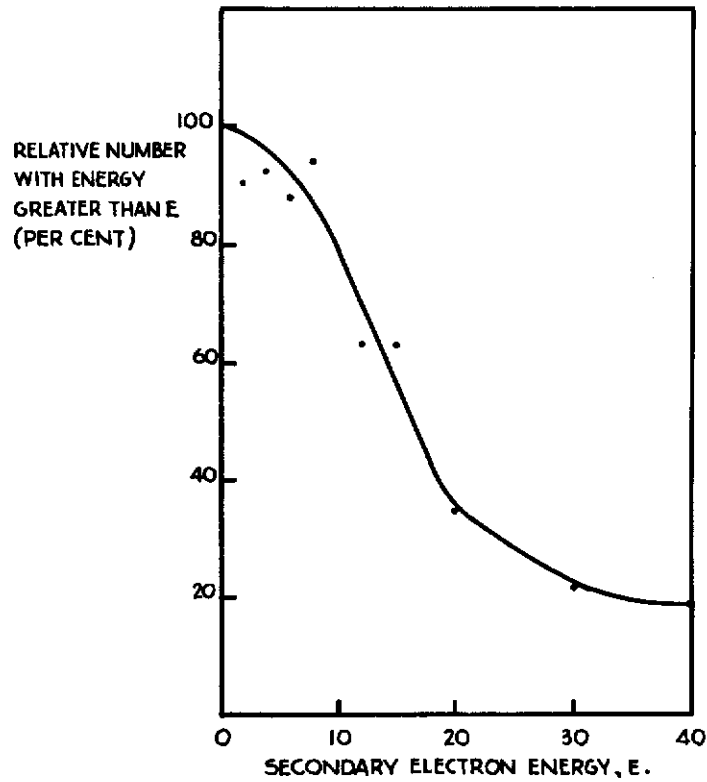


Figure 35 Secondary Electron Spectrum of Propane Using 1000 eV Primary Electron Energy.

# Contrails

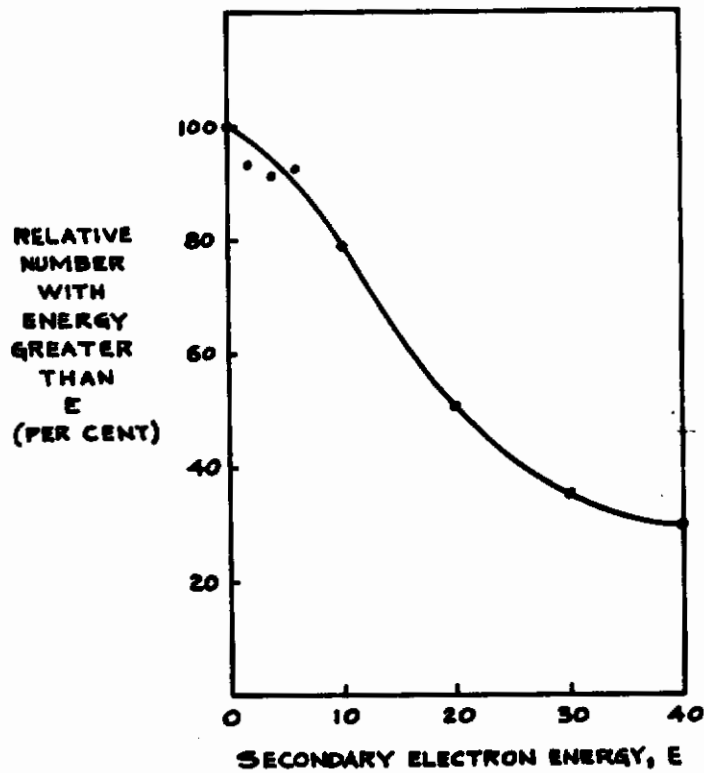


Figure 36 Secondary Electron Spectra of N<sub>2</sub> for Primary Electron Energy of 1000 ev.

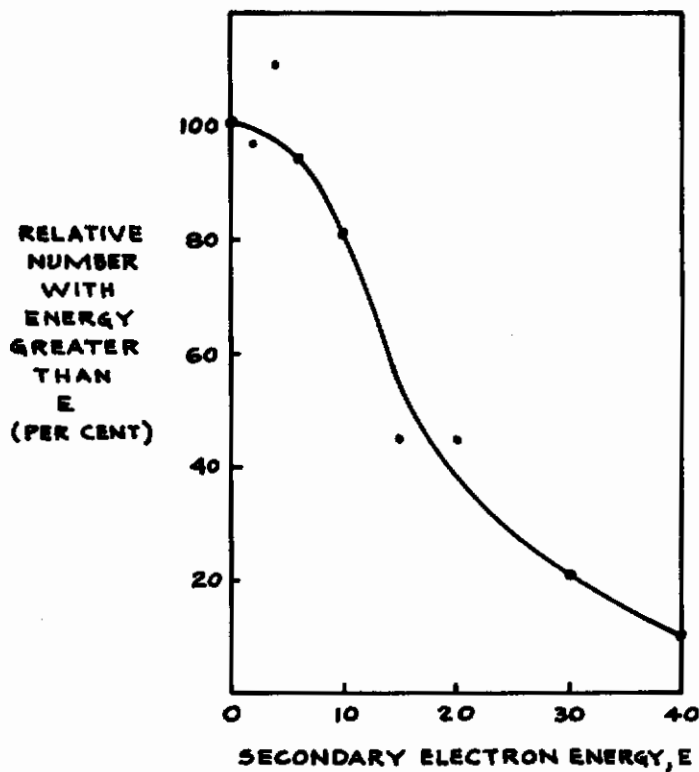


Figure 37 Secondary Electron Spectra of n-Butane for Primary Electron Energy of 1000 ev.

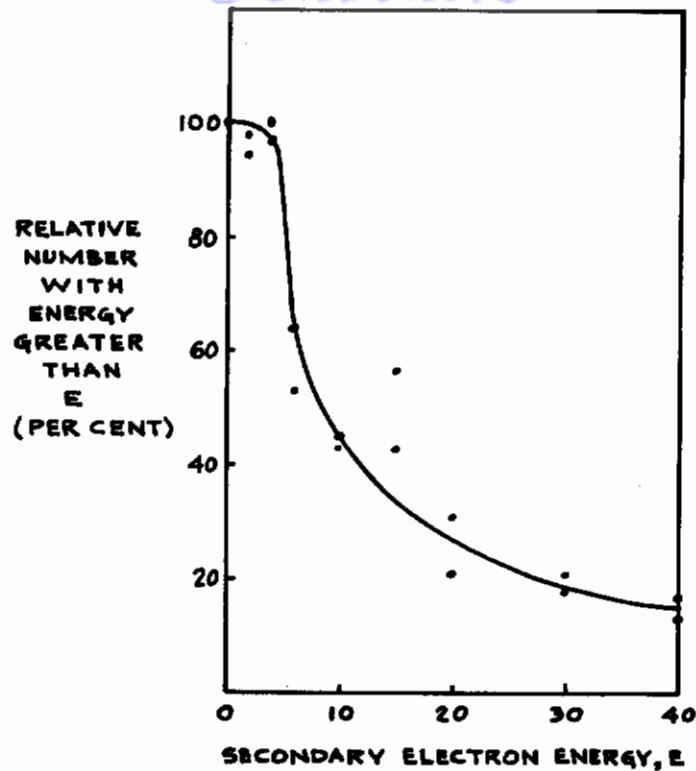


Figure 38 Secondary Electron Spectra of 1, 3-Butadiene for Primary Electron Energy of 1000 ev.

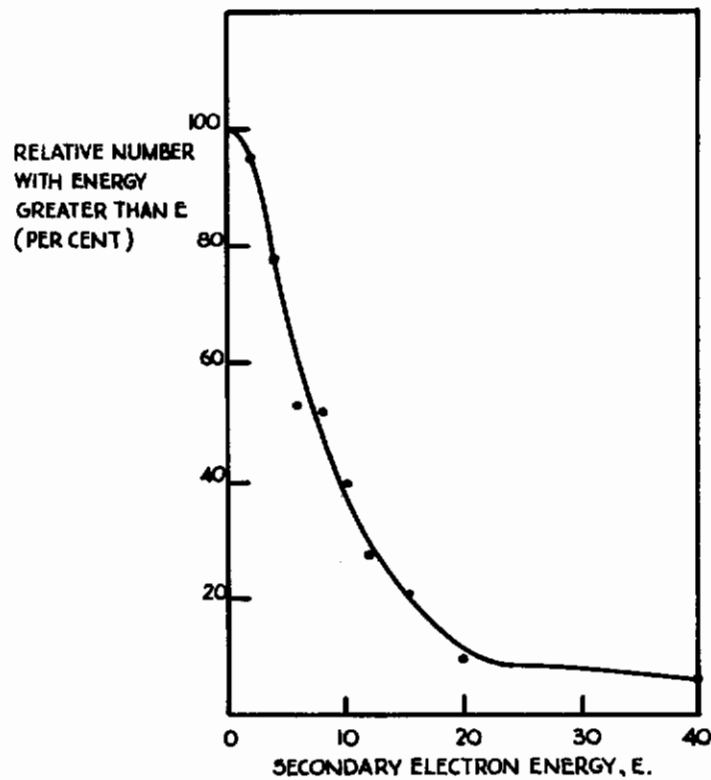


Figure 39 Secondary Electron Spectra of n-Pentane for Primary Electron Energy of 1000 ev.

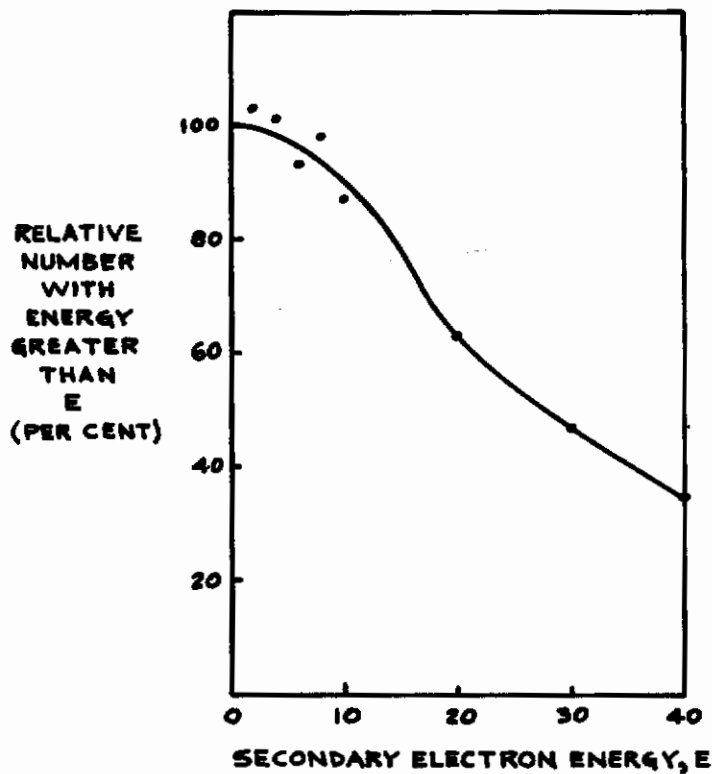


Figure 40 Secondary Electron Spectra of Argon for Primary Electron Energy of 1000 ev.

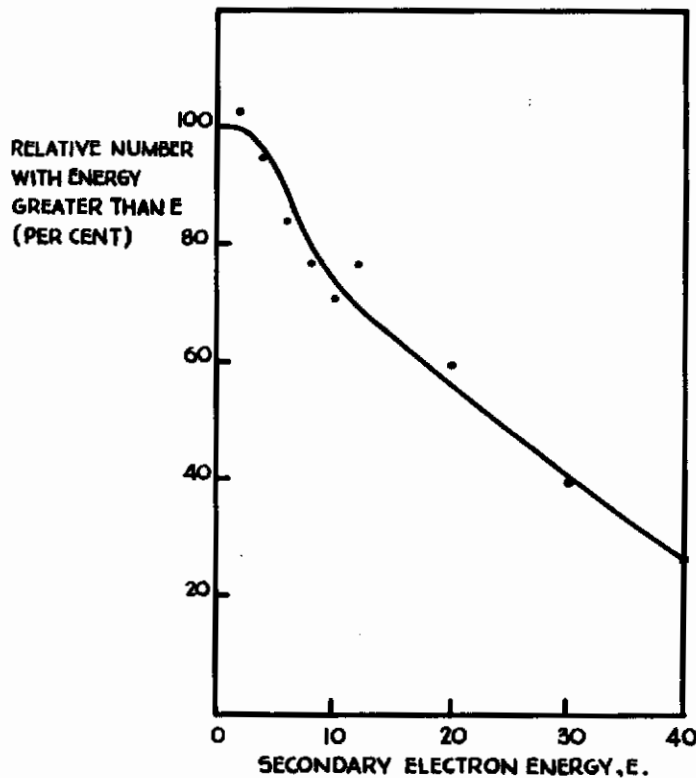


Figure 41 Secondary Electron Spectra of Cyclohexane for Primary Electron Energy of 1000 ev.



## V. INTERPRETATION AND EVALUATION OF THE DATA

A knowledge of the fraction of secondary electrons with sufficient energy to produce further ionization together with a detailed knowledge of their energy spectrum is of very basic importance to an understanding of the fundamental processes of radiation chemistry and radiation effects in materials.

The fraction of the secondary electrons with sufficient energy to produce further ionization for the several molecules studied with 1000 ev primary electrons is given in Table 14. It may be observed from the table that these fractions vary over a considerable range of values for the molecules studied.

An important independent experimental result with which the secondary electron energy measurements should be correlated is the measurement of the average energy,  $W$ , expended by an intermediate or high energy electron per ion pair formed in the gas. Since the quantity  $W$  depends on several parameters other than the fraction of secondary electrons which can cause further ionization, a simple linear correlation between  $W$  and the fraction of secondary electrons which can produce ionization is not to be expected. However, it seems probable that molecules which have large values of  $W$  relative to the ionization potential should tend to display relatively small values of the fraction of secondary electrons capable of ionization.

Table 14

Fraction of Secondary Electrons Exceeding the Ionization Potential of the Molecule for 1000 ev Primary Electron Energy.

<u>Molecule</u>	<u>Ionization Potential (1)</u>	<u>Fraction of Secondaries Capable of Ionization</u>	<u>W/I(2)</u>
N <sub>2</sub>	15.6	0.60	2.24
Argon	15.75	0.78	1.68
Propane	11.3	0.72	-
n-Butane	10.5	0.79	-
n-Pentane	10.5	0.36	-
1,3-Butadiene	8.8	0.48	-
Cyclohexane	9.5	0.75	-
Hydrogen	13.6	0.57(3)	-

(1) Units of Electron Volts.

(2) Section 2.16 of reference (9).

(3) Calculated using Born approximation for atomic hydrogen.

Unfortunately, the value of the mean energy loss per ion pair formed,  $W$ , has been measured only for N<sub>2</sub> and argon of the molecules for which secondary electron energy spectra have been measured. The value of  $W/I$  as reported by Platzman (9) for these two molecules are also given in Table 14. From these results the conclusion that  $W/I$  strongly reflects the effects of the fraction of secondary electrons capable of ionization seems to be valid. Additional meas-

urements of secondary electron spectra for molecules for which the W-values have been measured are necessary before this conclusion can be definitely substantiated.

Rigorous calculation of the secondary electron spectra of complex molecules is presently not feasible from basic quantum theory. Nevertheless, it is expected that the secondary electron spectra should be qualitatively similar to those calculable for atomic hydrogen. The differential spectrum for secondary electrons ejected perpendicularly to the primary electron beam for 1000 ev primary electrons was calculated in Section II of this report and is shown in Figure 26. The corresponding calculated integral spectrum is shown in Figure 42. The conditions for this calculation are essentially the same as the experimental conditions under which the secondary electron energy spectra were measured.

Comparisons of the secondary electron spectra measured for several molecules using 1000 ev primary electron energy (Figures 36 through 41) with the calculated spectrum for atomic hydrogen reveal that all of the measured spectra show the qualitative similarity with atomic hydrogen that was expected on theoretical grounds.

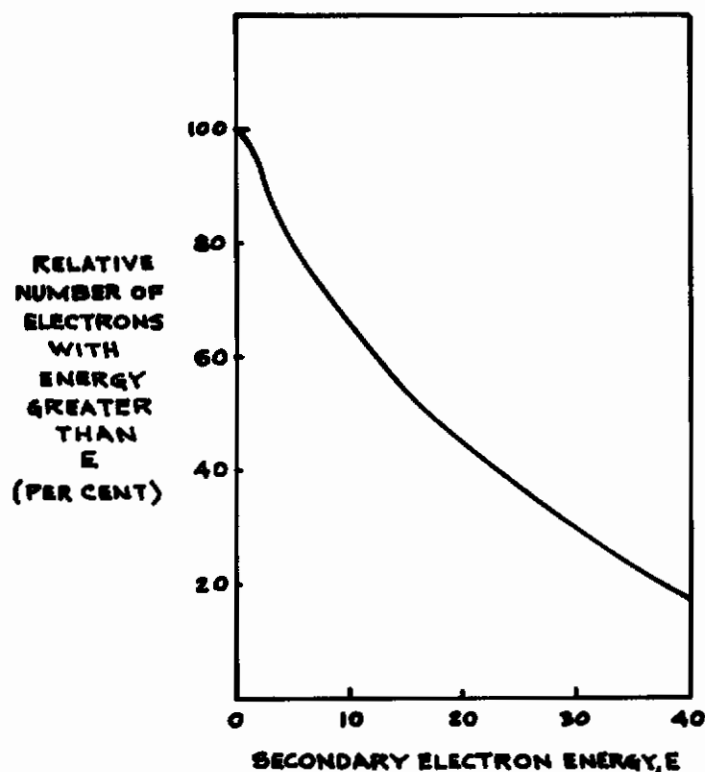


Figure 42 Calculated Integral Secondary Electron Spectrum for Atomic Hydrogen at a Primary Electron Energy of 1000 ev.

Due to the lack of independent experimental data and rigorous theoretical results with which these data might be correlated, more detailed interpretations and evaluations of these results are withheld until we have even more extensive

data. Some general conclusions are evident regarding the overall character of these measured spectra. The features of the secondary electron spectra which appear significant are the following:

- (1) The mean secondary electron energy of  $N_2$  is higher than that for propane at similar primary electron energies. In propane the molecule has a much larger number of energetically low-lying electronic states and hence it is to be expected that propane have a higher probability for ejection of low energy secondary electrons than does the nitrogen molecule.
- (2) For both  $N_2$  and propane the spectra show only a small shift with the change in primary electron energy in the energy range investigated. In both cases the small shift which is observed consists of a slight increase in the number of higher energy secondaries with an increase in primary electron energy. Since the primary energies used in these measurements were many times the ionization potentials, the rather slow increase in primary electron energy is consistent with theoretical treatments of ionizing collisions based on the Born approximation.

## VI. CONCLUSION AND FUTURE WORK

The successful modification of the coincidence mass spectrometer and the construction of the special x-ray tube for studies of x-ray ionization and fragmentation have been completed. Studies on x-ray ionization and fragmentations for several molecules have been presented. In addition, a number of secondary electron energy spectra for electron impact ionization have been measured.

Future work should extend these measurements to additional molecules of importance to radiation effects in materials. Also, the secondary electron energy spectra for x-ray ionization should be measured. In particular, emphasis should be placed on measurements of one or more groups of isoelectronic molecules. This emphasis should provide the necessary experimental information to allow important theoretical correlations and interpretations.

An important isoelectronic group for study is the series: ethanol, ethylamine, and propane. Each of these molecules contain 26 electrons. Although these are arranged so that there is an octet of outer shell electrons about each of the heavier atoms, there are varying numbers of non-bonding electron pairs. Theoretical correlations and interpretations of the experimental results should be made.

The present program represents the first study of x-ray ionization of gases in which mass analysis of the product ions has been conducted. For the first time, the fragmentation patterns resulting from inner shell ionization by x-rays have been measured. An important extension of this work could be achieved by employing a source of nearly monochromatic x-rays. This refinement would allow studies of x-ray ionization and fragmentation resulting from the impact of an x-ray photon with a well-defined energy. As a result, the theoretical interpretations would be greatly simplified, and the application of the data to the gross effects of radiation on materials would be direct.

However, obtaining a sufficiently intense source of nearly monochromatic, "soft", x-rays is a difficult experimental problem. Even with the extremely high sensitivity of the Coincidence Mass Spectrometer, the special x-ray tube was required in the present studies to obtain the necessary intensity of low energy x-rays for sufficient ionization in gases at pressures useable in a mass spectrometer. Any attempt to select a narrow band width from the x-ray spectrum by the techniques of x-ray crystal spectroscopy would considerably decrease the intensity. Nevertheless, the fundamental importance of the results which could be obtained by mono-energetic x-rays gives strong impetus to a search for an experimental solution.

## List of References

1. Steiner, B., Giese, C.F., and Inghram, M.G., J. Chem. Phys. 34, 1891, (1961).
2. Hurzeler, H., Inghram, M.G., and Morrison, J.D., J. Chem. Phys. 27, 313, (1957).
3. Weissler, G.L., Samson, J.A.R., Ogawa, M., and Cook, G.R. J. Opt. Soc. Amer. 49, 338, (1959).
4. Lossing, F.P., and Tanaka, I., J. Chem. Phys., 25, 1031, (1956).
5. Wiley, W.C., and Mc Laren, I.H., Rev. of Sc. Instr., 26, 1150-1157, (1955).
6. Daley, N.R., Rev. Sc. Instr., 31, 3, 264, (1960).
7. Waters, J.R., Nucl. Instr. and Methods, 7, 174-178, (1960).
8. Mott, N.J. and Massey, H.S.W., "The Theory of Atomic Collisions," Clarendon Press, Oxford, (1949).
9. Platzman, R.L., Chap. 2, "Radiation Biology and Medicine," Addison-Wesley, Reading, Mass., (1958).